A Survey on MIMO-OFDM Systems: Review of Recent Trends

Houda Harkat [1,2,*], **Paulo Monteiro [3,4]**, **Atilio Gameiro [3,4]**, **Fernando Guiomar [3]** and **Hasmath Farhana Thariq Ahmed [5,†]**

1   Centre of Technology and Systems (CTS), FCT Campus, NOVA University of Lisbon, 2829-516 Caparica, Portugal
2   Faculty of Sciences and Technologies, University of Sidi Mohamed Ben Abdellah, BP 2626, Route Imouzzer, Fes 30000, Morocco
3   Instituto de Telecomunicações, 3810-193 Aveiro, Portugal; paulo.monteiro@ua.pt (P.M.); amg@ua.pt (A.G.); guiomar@av.it.pt (F.G.)
4   DETI, University of Aveiro, 3810-193 Aveiro, Portugal
5   Department of Computer Science Engineering, Saveetha School of Engineering, Saveetha Institute of Medical and Technical Sciences, Saveetha University, Chennai 602105, India; hasmathfarhanathariqahmed.sse@saveetha.com or hasmath.farhana@vit.ac.in
*   Correspondence: houda.harkat@usmba.ac.ma
†   Current address: Vellore Institute of Technology, School of Computer Science and Engineering, Chennai 632002, India.

Abstract: MIMO-OFDM is a key technology and a strong candidate for 5G telecommunication systems. In the literature, there is no convenient survey study that rounds up all the necessary points to be investigated concerning such systems. The current deeper review paper inspects and interprets the state of the art and addresses several research axes related to MIMO-OFDM systems. Two topics have received special attention: MIMO waveforms and MIMO-OFDM channel estimation. The existing MIMO hardware and software innovations, in addition to the MIMO-OFDM equalization techniques, are discussed concisely. In the literature, only a few authors have discussed the MIMO channel estimation and modeling problems for a variety of MIMO systems. However, to the best of our knowledge, there has been until now no review paper specifically discussing the recent works concerning channel estimation and the equalization process for MIMO-OFDM systems. Hence, the current work focuses on analyzing the recently used algorithms in the field, which could be a rich reference for researchers. Moreover, some research perspectives are identified.

Keywords: cognitive radio networks; fifth generation 5G; multiple input output (MIMO); orthogonal frequency division multiplexing (OFDM); MIMO-OFDM

1. Introduction

Mobile devices have become very intelligent communication tools that behave as sensors in a cloud computing environment. Several enhancements have been applied to the core network to provide a high quality of service (QoS) and to handle novel diversified access technologies. With the introduction of the IEEE 802.22 norm, cognitive radio (CR) networks have become more relevant to the efficient management of the available spectrum resources, with less interference between adjacent users.

CR has the capability to change its parameters; so, it is possible for other users to access the available communication resources. Nevertheless, CR is only one functionality that software defined radio (SDR) offers as an emerging architecture concept.

Nowadays, multiple input multiple output (MIMO) systems have become a widely adopted technology; they are considered to be a strong candidate for 5G wireless communication systems.

The ascendant number of users and the necessity to increase the data rate have driven scientific and industrial collaborators to further boost the network capacity by adopting

several new technologies. Massive MIMO [1], is one innovative technology that consists of several antennas which enhance the spectral efficiency.

Moreover, Orthogonal Frequency Division Multiplexing (OFDM) combined with MIMO has given an interesting performance. MIMO-OFDM systems have drawn the attention of researchers over the last decade. Several MIMO-OFDM review papers and surveys, shown in Table 1, have been published to give a comprehensive analysis of the different challenging issues for the scientific community.

There were some papers proposing a simple overview of some important research axes and pointing out the recent technology evolutions [2] concerning MIMO systems, namely MIMO 5G candidate waveforms [3,4], channel models [5], and coding schemes [6] relative to MIMO technology. Other papers, which propose a deeper review of MIMO systems in general, are classified in Table 1 as well.

Table 1. Review paper concerning MIMO-SDR systems.

	Year	Details Paper Reference	Special Focus/General Vision of the Paper	MIMO-SDR System Research Axes
Simple overview	2019	Delson and Jose [2]	5G standards, specifications, and massive MIMO testbed, including transceiver design models using QAM modulation scheme	- Implemented massive MIMO testbeds - 5G specifications
	2017	Shafi, et al. [3]	5G standards, trials, challenges, deployment, and practice	- Channel characteristics and access - Waveforms for the 5G
	2014	Banelli, et al. [4]	Modulation formats and waveforms for 5G networks	- Waveforms for 5G networks including MIMO systems - MIMO channel effect
	2014	Wang, et al. [5]	Key technologies for 5G wireless communications	- 5G MIMO technologies - General view of MIMO channel models
	2012	Amin and Trapasiya [6]	Space–time coding scheme for MIMO system	- Time Coding Scheme
Deep review	2022	Our paper	MIMO-SDR OFDM systems	- New MIMO trends (hardware and architecture innovations) - MIMO waveforms - MIMO-OFDM systems advancements: channel estimation and equalization.
	2021	Chen, et al. [7]	Massive MIMO systems	- Algorithms for resource allocation - Channel estimation - Practical implementations

Table 1. *Cont.*

Year	Details Paper Reference	Special Focus/General Vision of the Paper	MIMO-SDR System Research Axes
2019	Mokhtari, et al. [8]	MIMO systems in presence of channel and hardware impairments	- MIMO waveform selection - MIMO hardware impairments - MIMO time varying channels
2019	Ijiga, et al. [9]	Channel estimation algorithms for 5G candidate waveforms	- MIMO channel estimation algorithms
2019	Wen, et al. [10]	5G massive MIMO localization	- MIMO channel models - MIMO channel parameter estimation - MIMO localization techniques
2015	Zheng, et al. [11]	Large-scale MIMO Systems	- Channel model - Main applications - Physical layer and network technologies
2015	Yang and Hanzo [12]	MIMO Detection	- Co-channel interference - MIMO detection - MIMO channel models
2008	Paul and Bhattacharjee [13]	MIMO channel modelling	
2002	Yu and Ottersten [14]	Models for MIMO propagation channels	
2018	Fatema, et al. [15]	Massive MIMO linear precoding techniques for single- and multi-cell systems	
2008	Garcıa-Naya, González-López and Castedo [1]	Overview of MIMO testbed technology	- MIMO developed testbeds

Only a few papers [8] discuss the waveforms tested using MIMO systems. Nonetheless, several authors [9–14] have analyzed the MIMO channel estimation and modeling problem. However, to the best of our knowledge, there has been until now no review paper that specifically discusses the recent works concerning channel estimation and the equalization process for MIMO-OFDM systems. The exception is that there are some review papers [16] on the MIMO-OFDM systems used especially for the underwater acoustic communication concept, where the transmission conditions are completely different to those of over-air transmission. In addition, there are some surveys of channel estimation and signal processing over massive MIMO systems [7]. Thus, there is a need for comprehensive review papers that analyze the current MIMO waveforms, channel estimation, and equalizations techniques. Therefore, the current paper gives a detailed overview of the recent advantages of MIMO systems in general and classifies the MIMO-OFDM waveforms, channel estimators, and equalizers. Figure 1 demonstrates the different research axes that will be discussed in the paper, in addition to the logical organization of the paper.
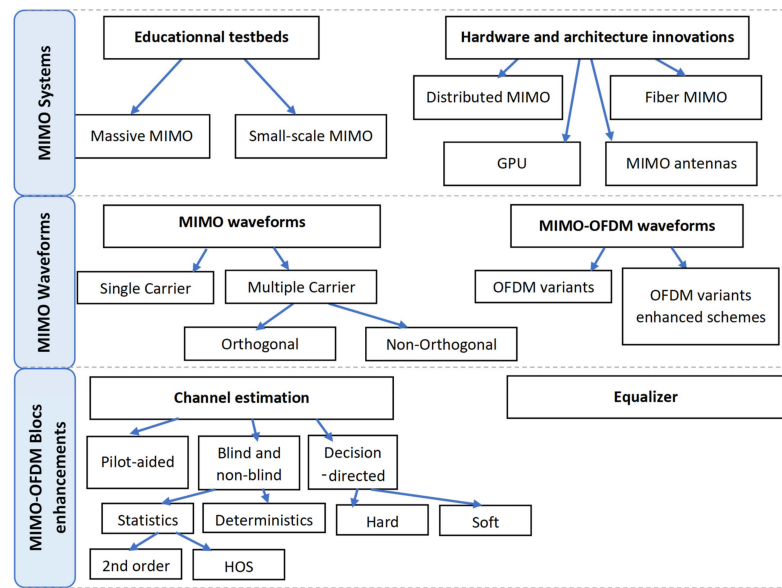
Figure 1. Overview of the discussed axes of the current review paper: in Section 3, three main axes will be analyzed: the MIMO systems' recent hardware and architecture innovations, MIMO waveforms, and MIMO channel estimation and equalization.

The rest of the paper is organized as follows: Section 2 gives an overview of the recent radio communication trends, namely SDR, CR, and MIMO. Section 3 describes the recent advances in the MIMO research field and the state of art concerning MIMO-OFDM systems. Finally, Section 4 summarizes the existing challenges and defines the novel research directions.

2. Overview of Recent Radio Trends

The CR, SDR, and MIMO systems are the key technologies in wireless communications. Those three radio trends have introduced a new design of cellular architecture to meet the 5G system requirements [5]. The next paragraphs give a brief insight into the CR, SDR, and MIMO systems.

2.1. Cognitive Radio Networks

The radio spectrum resources must be efficiently allocated and managed to assure the QoS for the end users while minimizing interference. Cognitive radio is an intelligent system which occasionally discovers an available spectrum part that can be allocated in a time/space and frequency manner. The spectrum allocation is time- and space-dependent, and therefore, the joint design of the routing and spectrum access is needed, with distributed implementation instead of the use of a common control channel.

The global architecture of a cognitive radio system is illustrated in Figure 2. It includes a cognitive unit that takes decisions based on various inputs and an SDR bloc whose operating software provides a range of possible operating modes.

The system also includes multiple sensors, a learning capability unit (external environment and an RF channel), and a virtual decision table (policy engine). In fact, the policy engine defines allowed/disallowed actions and sets the rules of communication (policies). The rules established must follow the telecommunication regularization defined by national or international organizations (namely the SDR forum): the spectrum, manufacturer, frequency band, ... [17].

It is extremely important to implement an efficient radio managing methodology which allows a continuous update of the policy rule definitions to meet the geographic location of the network and the radio standards. The policy engine is always controlling

the behavior of the cognitive radio system, and the policy changes must be validated by trusted entities that distribute the policies.
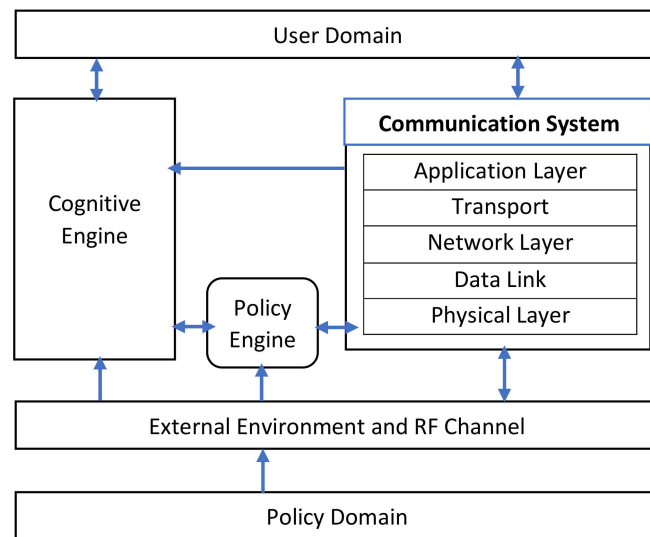
Figure 2. Cognitive radio network architecture.

2.2. System-Defined Radio Paradigm (SDR)

In SDR systems, several selected functions previously implemented at the hardware level have migrated to software blocs. In fact, SDR technologies implement wireless functionalities in programmable devices: the digital signal processor (DSP) and the field programmable gate array (FPGA). The implemented smart logic is further fused with modem software and radio frequency transceivers to manage the use of the available frequency spectrum and provide new innovative services to end users.

Figure 3 represents the architecture of an SDR transceiver. The SDR architecture is composed of a transmitter (Tx) and a receiver (Rx). The hardest things in the hardware part are the digital/analogue converter (ADC/DAC) relative sampling rate issues. To attain an optimal performance, the ADC/DACs are placed near an intermediate frequency section.

On the transmitter side, the incoming data are passed through a baseband signal processing block. Afterwards, the signals are modulated with an IF carrier signal; the IF signal is converted to an RF signal, and finally, it is transmitted to an antenna which will inject it into the communication channel.

At the receiver, the RF signal is filtered and down-converted into an IF signal. Subsequently, the IF signals are digitized, demodulated, and baseband-processed to finally extract the originally transmitted information.
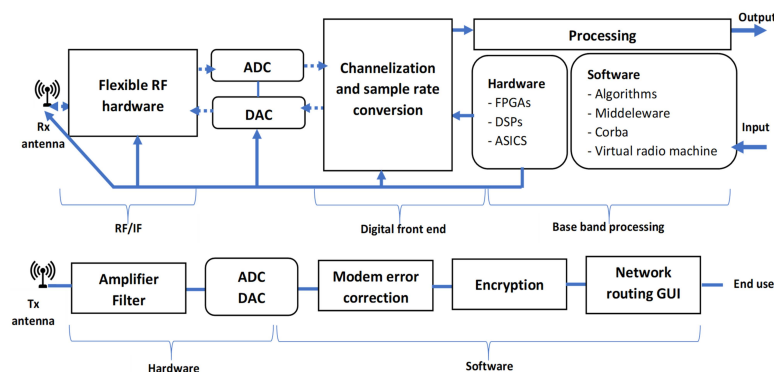
Figure 3. SDR architecture concept: the scheme clearly demonstrates the hardware and software parts that are fused together.

2.3. MIMO Systems

Let us consider the MIMO system model with N_t transmit and N_r receive antennas, as depicted in Figure 4.
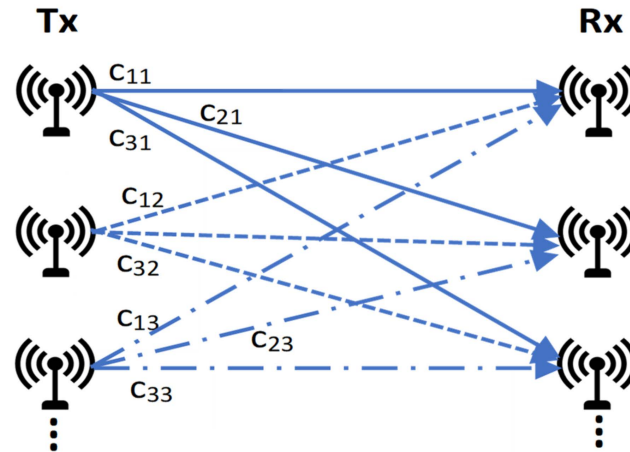
Figure 4. MIMO system Model.

The channel is modeled as an $N_t x N_r$ matrix; the received signal y is expressed as:

$$y = Cx + n \tag{1}$$

where x is the transmit signal vector, and C and n are the fading channel matrix and the noise vector, respectively.

The ergodic channel capacity of the system, in ideal conditions, is:

$$Capacity_{ideal} = E\left[\max_{Q,\, tr(Q)\leq 1} \log_2 det\left(I + \rho CQC^H\right)\right] = E[\log_2 det(I + \rho DSD)] \tag{2}$$

where $()^H$ is the Hermitian transpose and ρ is the signal to noise power ratio (SNR).

Q is the optimal signal covariance, formulated through a singular value decomposition of the matrix C and an equalization process, as follows:

$$\begin{cases} SVD(C) = UDV^H \\ Q = VSV \\ S = [s_1,\, \ldots, s_{min}(N_t, N_r), 0, \ldots, 0] \\ s_i = \left(\varepsilon - \frac{1}{\rho d_i^2}\right)^+,\ i = 1, \ldots,\ min(N_t, N_r) \end{cases} \tag{3}$$

d_i are the diagonal elements of D, and ε is chosen $s_1 + \ldots + s_{min}(N_t, N_r) = N_t$.

We note that if $s_i \leq 0$, it is automatically rounded to zero.

In the case where the transmitter has only statistical CSI, the ergodic capacity diminishes as the Q could be optimized from the sense of mutual information:

$$Capacity_{statistical\ CSI} = \max_{Q} \log_2 det\left(I + \rho CQC^H\right) \tag{4}$$

If the transmitter has no CSI, the capacity maximization could be on the basis of Q, which is expressed in this case by:

$$Q = \frac{1}{N_t I} \tag{5}$$

The capacity, in this special case, will be given by:

$$Capacity_{no\ CSI} = E\left[\log_2 det\left(I + \rho CQC^H\right)\right] \tag{6}$$

3. State-of-the-Art MIMO-SDR Systems

In this section, we will discuss the main innovative work concerning MIMO systems: the hardware/software, the different existing waveforms, the channels, and the equalization algorithms.

3.1. MIMO Systems

The work conducted in this general area could be broadly classified into two groups: the platforms and testbeds developed for educational purposes and the innovation introduced in the hardware/architecture implementation.

3.1.1. Educational Platforms and Testbeds

Multi-user MIMO systems (MU-MIMO) are simple systems which use multi-antenna base configurations to serve a multitude of users but could not handle the performance offered by the massive MIMO systems. The research work available in this category is split into two groups: massive MIMO systems and small-scale MIMO systems.

Massive MIMO Systems

One of the first fully validated and functional massive MIMO testbeds is proposed in the context of a collaboration between the University of Bristol and Lund University, associated with National Instruments (NI) [18]. The MIMO-OFDM system is designated for the evaluation of spectral efficiency [2]. It is operable in the frequency band of 1.2–6 GHz, with a bandwidth of 20 MHz and a sampling rate of 30.72 MS/s. In addition, it supports 128 antennas and maximum of 10 users per time/frequency slot. The duration of a time slot is 0.5 ms, and the number of used subcarriers is 1200, with a 145.6 bits/s/Hz spectral efficiency [2,18].

In the same context, Hasan, et al. [19] have suggested another hardware testbed with a base station of 128 antennas serving 22 users, with a spectral efficiency value of 145.6 bis/s/Hz.

A receiving patch antenna array placed at 24.8 m away from the transmitting antenna array of 128 elements was arranged in front of the base stations. The time-division duplex (TDD) massive MIMO system operates at a carrier frequency of 3.51 GHz with a 256-quadrature amplitude modulation (QAM) scheme.

The channel estimation was performed in a cyclic manner every 5 ms, and a zero-forcing (ZF) or Minimum Mean Square Error (MMSE) was used to assure a reliable data transmission.

Hasan, Harris, Doufexi and Beach [19] conducted some experiments to assess the system behavior for a high number of users (>22), spatially multiplexed within a single base station.

The authors realized that within the 23rd user addition the constellation diagram deteriorated, whatever the position of this user was. This behavior was justified by the CSI estimation accuracy.

In addition, another massive MIMO-SDR system with time-division multiple access (TDMA) was proposed [20], at the Tennessee Technological University, that supports up to 70 nodes and 30 × 30 antennas (i.e., 30 Universal Software Radio Peripherals (USRPs)). The system capacity and transmission rates were measured using the Vandermonde channel estimation model [21,22]. The authors proved that, by slightly adjusting the range of the arrival angles and the base station antenna distance, the model became more adequate for the outdoor environment with high loss propagation conditions. They remarked that the channel capacity measurement grew linearly with the deployment of more antennas in the base station.

LuMaMi [23], the famous Lund University massive MIMO OFDM testbed, is able to handle up to 100 antennas (i.e., 50 USRPs) with a bandwidth of 20 MHz. The MIMO coding and decoding processes were implemented in 50 FPGA devices of the Xilinx Kintex-7 type. This system's main features are:

- It allows the amount of data supported in both the uplink and the downlink to be 384 Gbits/s.
- The synchronization is performed with an external signal derived from 8 Octo-Clock devices (7 Octo-Clock devices commanded with a master Octo-Clock). However, some phase tight distortion appears during the transmission tests performed between the base station radio frequency channels; this is due to the receiver channels [24].
- The system could be extended up to 128 antennas.
- A planar T-shaped antenna array with 160 dual polarized elements was used. Moreover, five USRP-RIO-type 2953Rs are deployed to emulate the receiving user equipment with a GPS reference signal connection capability.

Another famous massive MIMO LTE system testbed is the OpenAirInterface [25] testbed, which is relatively smaller than the ones already discussed. The platform applies a time-division duplex (TDD) reciprocity channel calibration to obtain accurate CSI channel information. It supports up to 64 antennas with a bandwidth of 5 MHz, a center frequency of 2.6 GHz, and a sampling rate of 7.68 MS/s. In addition, the number of used subcarriers is 300, the duration of one time slot is 0.5 ms, and the maximum number of simultaneous users is four.

Malkowsky, et al. [26] focused on designing a framework for a massive MIMO testbed by taking into consideration some basic requirements, mainly the system complexity, the signal waveform mode, and the frame format. The design was validated within the Lund University massive MIMO hardware [23]. The suggested design supports up to 100 antennas and more than 50 FPGAs. It is allowable to have up to 12 users at the same time/frequency slot with an OFDM modulation in a time-division duplex (TDD) (LTE-like TDD) strategy [26]. The tests were performed in indoor and outdoor environments.

Finally, a mm-wave MIMO testbed [27] was developed at the Institute of Digital Signal Processing (DSV) at the University of Duisburg-Essen to operate, in the beginning, for sub-6 GHz frequencies. It was implemented in a heterogenous environment, over the FPGA, DSP, and GPU.

The platform could be reached remotely through VPN by academic and industrial researchers.

Small-Scale MIMO Systems

Several additional studies could be classified as being in the educational platform and testbed category, which is mainly designated for a general and a fast prototyping of MIMO systems with more simple architectures (maximin 4×4 systems) and high performance.

Table 2 regroups the most successful testbeds implemented in the literature. A detailed description is given in terms of architecture, software, hardware composition, and spectrum division.

Table 2. Small-scale MIMO systems characteristics.

Testbed [1]	Year	Tx × Rx [2]	Hardware Implementation		Software [3]	BW [4]	Operating Frequency	Waveform
			DSP	FPGA				
Zamfirescu, et al. [28]	2019	2 × 2/3 × 3	——	- ADS62P44 ADC converter	GNU radio	——	2 GHz	OFDM
Ribeiro and Gameiro [29]	2017	2 × 2	DSP48	- Xilinx Virtex6 (COTS Xilinx ML605 board motherboard) - Analog Devices AD FMCOMMS1-EBZ daughterboard.	MATLAB	Max61.44 MHz	400 MHz–4 GHz	- OFDM with 256-QAM modulation - 800 used subcarriers out of 1024
Vielva, et al. [30]	2010	4 × 4	MAX2829 single chip RF transceiver		MATLAB	Up to 40 MHz	2.412–2.472 GHz and 5.15–5.35 GHz	OFDM 802.11 WLAN
GTEC [31]	2010	2 × 2/4 × 4 2 × 3	Texas Instruments TMS320C6416 DSP running at 600 MHz	Xilinx Virtex II XC2V1000–6	3L Diamond software	20 MHz	2.4 GHz 5.2 GHz	16 QAM modulation
Bates, et al. [32]	2008	4 × 4	Texas Instruments DSP development kit: 440 Logic Elements 9-bit DSPs	Altera Stratix II EP2560 2.5 Mb Memory 60	MATLAB	Up to 40 MHz	The 2.4 GHz to 2.5 GHz	OFDM with 64-QAM modulation
GEDOMIS [33]	2006	4 × 4	Multi-DSP processing board, Pentek, model 4292, provides four fixed-point DSPs, operating, Texas Instruments model TMS320C6203, at 300 MHz in a single-slot VME motherboard.	8 FPGAs: six Spartan-II and two Virtex-II	——	——	2.412–2.472 GHz and 5.15–5.35 GHz	- OFDM based on IEEE 802.11 g/a physical layer - 64-QAM modulation
GTAS by Ramirez, et al. [34]	2006	2 × 2	An SMT365 module contains a DSP at 600 MHz with 1 MB of internal memory	Xilinx Virtex-II Pro X2VP7	MATLAB	Up to 20 MHz	The band around 2.4 GHz	Quadrature Phase Shift Keying (QPSK) modulation and Alamouti space–time coding
Vienna [35]	2006	4 × 4	FPGA boards from Sundance [36]: equipped with a fixed-point DSP (600 MHz, 4800 MIPS peak performance, Texas Instruments TMS320C6416), a Xilinx FPGA (Virtex II XC2V1000-4-FF896), and 8 Mbytes of RAM		MATLAB	20 MHz	2.45 GHz	4-QAM/16-QAM constellation
Roy and Bélanger [37]	2006	4 × 4	C6701 [1]	Virtex II [1]	——	40 MHz [1]	——	——

Table 2. *Cont.*

Testbed [1]	Year	Tx × Rx [2]	Hardware Implementation		Software [3]	BW [4]	Operating Frequency	Waveform
			DSP	FPGA				
SABA by Borkowski, et al. [38]	2006	4 × 4	___	The BenBLUE II (BigBlue) module is equipped with two XC2V3000 Virtex II FPGAs	___	30 MHz	10.525 GHz, following the IEEE 802.16 standard	OFDM with 16-QAM modulation
STAR [39]	2006	TR-STBC: 2 × 1 DFE-MIMO: 4 × 4 OFDM-MIMO: 4 × 4	- Nine FPGAs per 12-channel platform - The authors had written a short review about the FPGA and DSP devices available at that time. However, we could not identify which ones were used.		MATLAB or octave	2 MHz 1 MHz 15 MHz	2.0–2.7 GHzcentred on 2.45 GHz	BPSK π/4 DQPSK 64-carrier QPSK
STARS [40]	2005	2 × 4	Sundance's signal processing modules are based on XILINX Virtex II/Virtex II-pro FPGAs and Texas Instruments' TMS320C6416 DSPs		MATLAB	Up to 30 MHz	2.4 GHz band	___
UCLA2 [41]	2005	4 × 4	Pentek 4291 Quad DSP [(TMS320C6701)]/Pentek 4292 Quad DSP [(TMS320C6203)] processing boards	Xilinx Vertex II X3000 FPGA	MATLAB	Up to 20 MHz		OFDM with 64-QAM modulation
Wallace, et al. [42]	2004	4 × 4	Base on Pentek DSP platform: four separate TI TMS320C6203 fixed-point DSPs	___	MATLAB		2.45 GHz	4-QAM constellation
UCLA [43]	2004	2 × 2/4 × 4	___	___	MATLAB	25 MHz	5.25 GHz	OFDM with 4/16/32-QAM constellation
Morawski, et al. [44]	2003	4 × 4	___	___	___	Up to 3.5 MHz	1.88756 Hz	OFDM with 64-QAM modulation
Rice Murphy, et al. [45]	2003	2 × 2	XtremeDSP Kit FPGA board (XC2V2000 Xilinx Virtex II FPGA)		___	Up to 20 MHz	From 900 MHz to 2.6 GHz	802.11b wireless LAN standard
Fabregas, et al. [46]	2003	2 × 2	___	A 1.5M gates ALTERA EP20K1500EBC652-1X	MATLAB	20 MHz	5.15 GHz and 5.35 GHz	OFDM with 16-QAM modulation

[1] Testbed name if it exists, and contributors' names; [2] Refers to system architecture; [3] MATLAB, LabVIEW, or GNU radio; [4] BW: Bandwidth.

Many of those testbeds have memory buffers accessible in real time, and both their analogue digital converters (ADCs) and their digital analogue converters (DACs) offer a 12-bit resolution and a sampling rate of more than 50 Msamples/s.

In addition to MathWorks, the TI Code Composer is used to develop some of the described testbeds. Additionally, the FPGA code is created within some Xilinx FPGA tools such as ISE or System Generator. The platforms built with Sundance hardware (Sundance Multiprocessor Technology Ltd., Chesha, UK) [36] adopt 3L Diamond.

3.1.2. Hardware and Architecture Innovations

From a hardware point of view, in the beginning the MIMO systems were adopting very simple architectures from 2 to 4 USRPs [29,34]; afterwards, massive MIMO systems [18,23] appeared with a capability to serve a high number of end users (22–24 users). Thus, novel architectures were nominated, particularly distributed MIMO [47,48], fiber-based systems [47], and GPU implementations. In addition, some antenna prototypes were especially designated for MIMO-SDR technology.

Distributed MIMO

The distributed MIMO system [47,48], as the name indicates, uses distributed antennas, interconnected via wireless or wired together. Distributed architectures offer multiplexing capability and macro-diversity gains. However, to exploit the full gains offered by such a MIMO system, it is necessary to deploy the channel resources to behave as multiple-antenna arrays. There are two possible architectures that such systems could have [48]:

- Single source transmission: a source (S), generating the signals to be transmitted, is connected via wireless or a physical interface to the non-collocated transmitting antennas. The signal is received, in the other side, by another set of antennas and transmitted to a receiving point (R) that gathers all the information. The signaling channel interfaces are necessary to set up the MIMO communications. Please refer to Figure 5a.
- Cooperative transmission: in this case, each transmitting antenna represents a signal source by itself. The transmitting and receiving antennas can cooperate, using signaling channel information, without the need of an intermediate point. Please refer to Figure 5b.
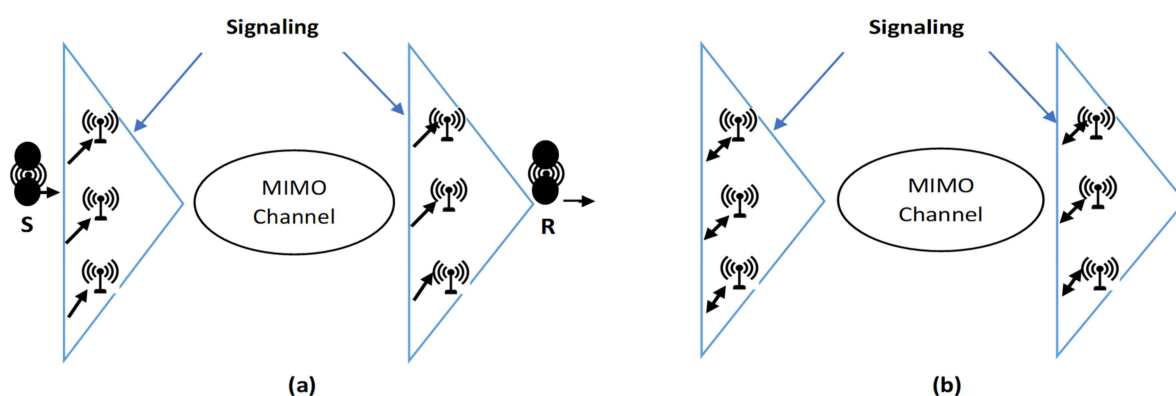
Figure 5. Distributed MIMO system possible architectures: (**a**) single source transmission and (**b**) cooperative transmission. The signaling interface, in the transmission and reception side, is assigned to establish the MIMO transmission channel.

We note that the signaling channel (in the transmitter and the receiver side) could be at the same time/frequency band of communication; it is in-band. Otherwise, it is out-of-band, i.e., over an orthogonal channel [48].

Fiber-Based Systems

In analogue radio over fiber, the analog up-converted radio frequency signal is transmitted through optical fiber and converted back to electrical after the transmission. The up-conversion and the phase synchronization are performed by several conventional transmitters with less complexity. Nevertheless, this transmission technique is affected by the distortion and nonlinearities of the optical transmission cables.

However, recent advances [47,49,50] show a combination of fiber-based technology with distributed MIMO systems. A low-cost [47,50] testbed was proposed to allow researchers to further investigate in this axis.

The distributed MIMO testbed based on high-speed sigma–delta-over-fiber [47] corrects the problem of phase coherence between multiple distributed access points. The testbed with a central unit feeding twelve access points has been built with a low-cost fiber connection. Initial experiments at a center frequency of 2.365 GHz are presented in [47].

Another 3×3 testbed was proposed by Gordon, Crisp, Penty and White [50]. The system architecture, composed of twenty users and three base stations, draws a 259 bit/s/Hz median aggregate capacity in line-of-sight (LOS) and 233 bit/s/Hz in no LOS propagation conditions.

GPU Implementations

The traditional MIMO-SDR testbeds are implemented over DSP and FPGA boards. Although DSP and FPGA provide code flexibility and high performance, they present some drawbacks for some applications:

The DSP arithmetic function does not support the new telecommunication trends.

Developing and debugging FPGA is very complex and requires a prior advanced knowledge about the environment.

Recent scientific investigations are focused on the parallelization of signal-processing code blocks using GPUs to achieve a higher processing speed for the SDR testbeds. The CUDA programming model, based on C, offers high-speed arithmetic processing with great flexibility.

Several research works have been published in this area, proposing a complete SDR platform [51,52] or only a partial process [27,53–55] implemented over a GPU.

Ahn, Kim, Ju, Choi, Choi and Choi [51] use CUDA SDK to implement the signal-processing blocks of a 2×2 WiMAX MIMO system over an NVIDIA GTX275 GPU, (Santa Clara, CA, USA). The computational performance was compared with an implementation based on TI TMS320C6416 DSP, which shows that the computation time using a GPU is 3–16 times faster than the DSP. The total computational time for every single WiMAX frame (of 5 ms duration) is 4.346 ms.

However, Han, Jin, Ahn, Choi and Hyeon [52] present another MIMO system, a 4×4 3GPP (3rd Generation Partnership Project) TDD LTE-A (Long Term Evolution-Advanced), implemented over a GPU. Two NVidia's GeForce GTX Titan GPUs were used, one for the uplink data and the other one for the downlink data. Figure 6 illustrates the system architecture which includes four transmitting and receiving antennas at the base station site and two pieces of end-user equipment.

Roger, Ramiro, Gonzalez, Almenar and Vidal [53] propose a heterogeneous MIMO system with a maximum likelihood (ML) signal detector implemented over a GPU, namely a sphere decoding algorithm. A bit-interleave-coded modulation (BICM) [56] was adopted, while, Wu, Sun, Gupta and Cavallaro [54] chose a completely novel multi-pass trellis traversal (MTT) detection algorithm, implemented over an NVIDIA GPU, that performs similarly to already existing algorithms.

Gokalgandhi, Segerholm, Paul and Seskar [55] use a GPU for accelerating the Least Squares (LS) channel estimation algorithm and the demodulation of the uplink OFDM single-user MIMO system. The implementation was realized in an ORBIT testbed [57], where the performance of the system was tested using different configurations depending on the number of antennas and the Fast Fourier Transform (FFT) length. The authors

conclude that the performance offered by a GPU is limited when increasing the number of antennas and the FFT length. Thus, in a following work they suggested parallelizing the implementation and using distributed algorithms and a distributed server.
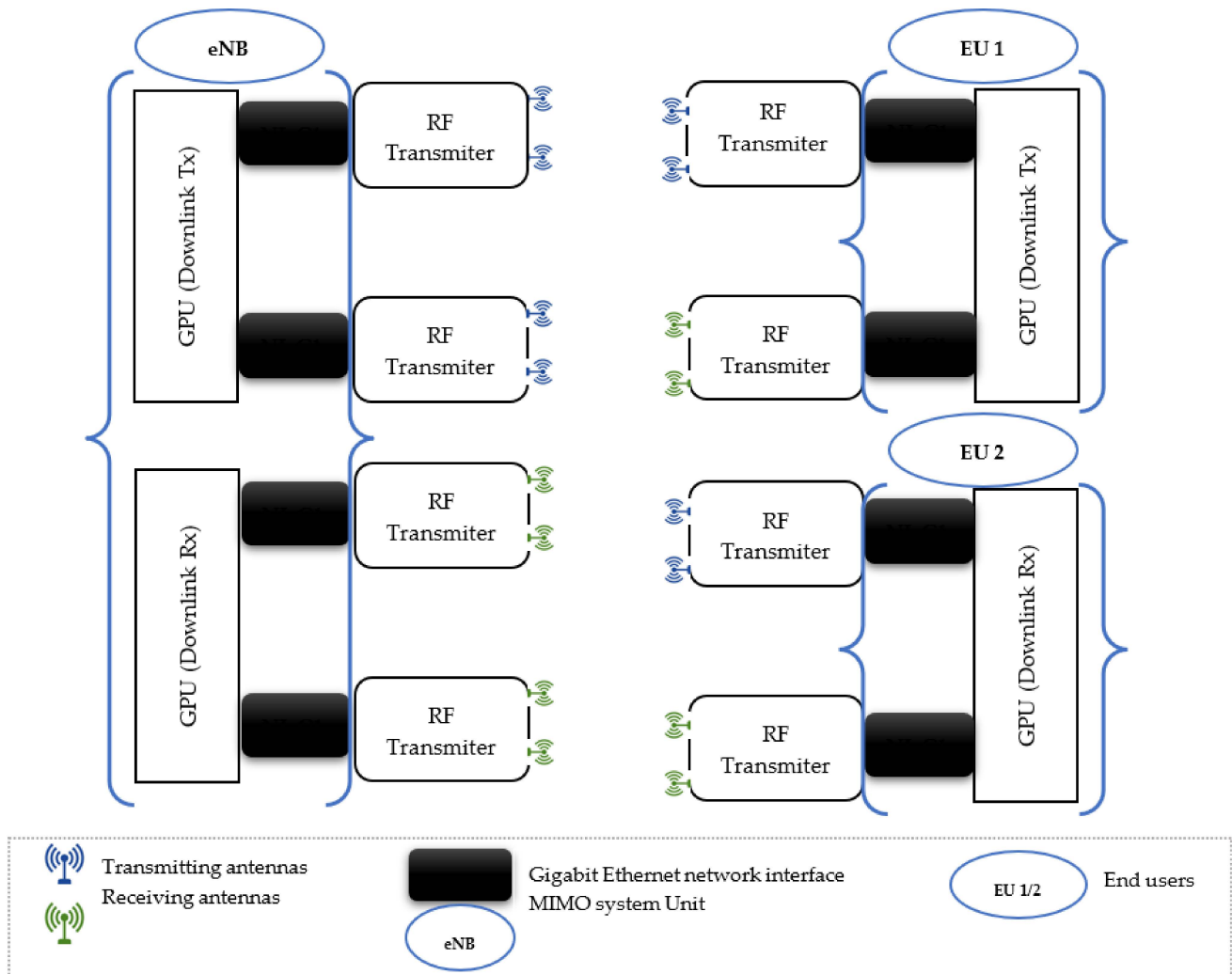
Figure 6. 4×4 3GPP TDD LTE-A MIMO system architecture.

Another heterogeneous MIMO system was designed [27] to accelerate the logic treatment. This is the mm-wave testbed, which uses open computing language (OpenCL) to transfer data between the FPGA and GPU without involving the CPU.

MIMO Antennas

At this point, the researchers have been focused on designing a new antenna with a maximum gain and lower loss. There were some array antenna prototypes designed to work with base stations [58] and others for the end user's deployment [59]. The main innovation concerning this research axis is the concept of reconfigurable antennas [60,61]. Reconfigurable antennas could change their operation frequency, in addition to their characteristics, to operate within multi-mode services and standards. Thus, they offer multiple advantages such as:

- Operability in multi-band frequencies
- Polarization diversity
- Low size and cost with high performance.

In fact, increasing the number of active elements used by the antennas allows more reconfigurable features (frequency, bandwidth, . . .). To obtain this reconfigurable capability, it is necessary to deploy some micro-electronical components such as micro-electromechanical systems (MEMS), varactor, and PIN diodes.

Kamran Shereen, Khattak and Witjaksono [60], Ojaroudi Parchin, Jahanbakhsh Basher-lou, Al-Yasir, Abd-Alhameed, Abdulkhaleq and Noras [61] did an extensive review about reconfigurable antennas for 5G applications in general. They cited and analyzed several prototypes recommended for MIMO and cognitive radio systems [62–66].

3.2. MIMO-SDR Waveforms

3.2.1. MIMO Waveforms Analysis

The waveforms implemented within MIMO systems could be coarsely classified into two categories: single-carrier waveforms and multi-carrier waveforms. In addition, multi-carrier waveforms are divided into two subgroups: orthogonal and non-orthogonal ones. Table 3 regroups the waveform classification with the relevant references. The table summarizes the main advantages and drawbacks of every waveform when deployed with MIMO systems.

Table 3. MIMO waveforms classification: single-carrier and multi-carrier spectrum access techniques.

		Waveform		Reference	Advantages/Disadvantages/Summaries
		Name	Acronym		
Single-Carrier		Single-carrier QAM	SC-QAM	[67]	- Even though it requires very low computational resources, it is not really adapted to MIMO systems - Less flexible in spectral allocation
		Single-carrier transmission with frequency domain equalization	SC-FDE	[68–70]	Considered as a direct alternative to OFDM as it overcomes the drawbacks presented by this technique. However, it does not offer the same flexibility given by OFDM concerning the management of the bandwidth and the energy resources.
		Single-carrier frequency division multiplexing	SC-FDM	[71,72]	SC-FDM has a low Peak-to-Average Power Ratio (PAPR) compared to OFDM. However, it suffers from noise enhancement [72,73] phenomena.
		Single-carrier FDP	SC-FDP	[70,74,75]	SC-FDP has lower PAPR in comparison with OFDM for a low number of end users. However, with a higher number of end-users SC-FPD performs the same as OFDM [70].
		Single-carrier frequency division multiple access	SC-FDMA	[76,77]	Presents some disadvantages compared to OFDM: - As the data on each frequency are not orthogonal, the channel estimation using pilots is complex. - Deploying a non-linear detection algorithm is very complex. 1. In an outdoor environment, OFDM performs better than SC-FDMA.
Multi-Carrier	**Orthogonal**	Orthogonal frequency division multiplexing	OFDM	[78]	This waveform has some drawbacks: - High PAPR. - Intolerance to the nonlinearities of the power amplifiers. - High sensitivity to carrier frequency offsets and transmitted signal fluctuations.
		orthogonal frequency division multiple access	OFDMA	[76,77]	- higher spectral efficiency for MIMO systems. - Inter-symbol interference (ISI) does not exist.
		Rate-splitting multiple access	RSMA	[79]	RSMA is a robust technique that allows the deploying of more powerful coding approaches [80].
		Multi-carrier code division multiple access	MC-CDMA or OFDM-CDM	[81]	- high presence of PAPR - Improves OFDM but introduces some other phenomena: bit error rate (BER) degradation and apparition of out-of-band interference (OBI)

Table 3. *Cont.*

Waveform			Reference	Advantages/Disadvantages/Summaries
	Name	Acronym		
Non-Orthogonal	Sparse code multiple access	SCMA	[82]	- For small number of end-users, SCMAs have a lower complexity. - Higher PAPR compared with SC-RSMA. - Offers a very low density spreading, requires synchronous multiplexing and iterative joint detection. - SCMA does take advantage of the fully available diversity; it uses only a portion of the time/frequency slots. - For end users deploying different spreading factors, SCMA is not a good candidate.
	Filter Bank Multi-Carrier	FBMC	[83]	- It is an OFDM evolution. - The existing research papers show that it is poorly compatible with MIMO systems [84]. - It is not an attractive candidate for 5G systems.
	Space Division Multiple Access	SDMA	[85]	- High overloading factor. - Robust blind detection.
	Multi-User Shared Access	MUSA	[86]	- Higher PAPR
	Nonorthogonal multiple access	NOMA	[87]	- Users are superimposed in the spectral domain, they could share the same frequency bin in the same time instance.

As OFDM is a strong candidate for fifth-generation (5G) telecommunication systems [80] and it is the most popular waveform used for MIMO systems, an additional OFDM derivative waveform will be introduced in the next section.

However, the OFDM-MIMO system model is introduced in detail in the following. The theoretical foundation corresponding to every waveform is described in the attached references.

This section may be divided by subheadings. It should provide a concise and precise description of the experimental results and their interpretation, as well as the experimental conclusions that can be drawn.

3.2.2. OFDM/Cyclic Prefix OFDM (CP-OFDM) Theory Aspects

The OFDM transmitter scheme (please refer to Figure 7) is composed of several signal-processing blocks: inverse fast Fourier transform (IFFT) processing, cyclic prefix (CP) insertion, and spectrum enhancement. Serial to parallel block converts several consecutives bits to parallel streams with a low bit rate. The modulation (or symbol mapping) is conducted with QAM, QPSK, or Binary Phase Shift Keying (BPSK). In the receiver side, we have inverse operations to decapsulate the signal, including fast Fourier transform (FFT) processing and cyclic prefix removal. Additional processing is required to estimate the channel effect and to allow a synchronized communication between the transmitter and the receiver. The cyclic prefix insertion and the removal blocks are more appropriate to the cyclic prefix OFDM (CP-OFDM) scheme. Additionally, the filtering block in the transmitter and receiver parts exist in the filtered OFDM (F-OFDM) version.
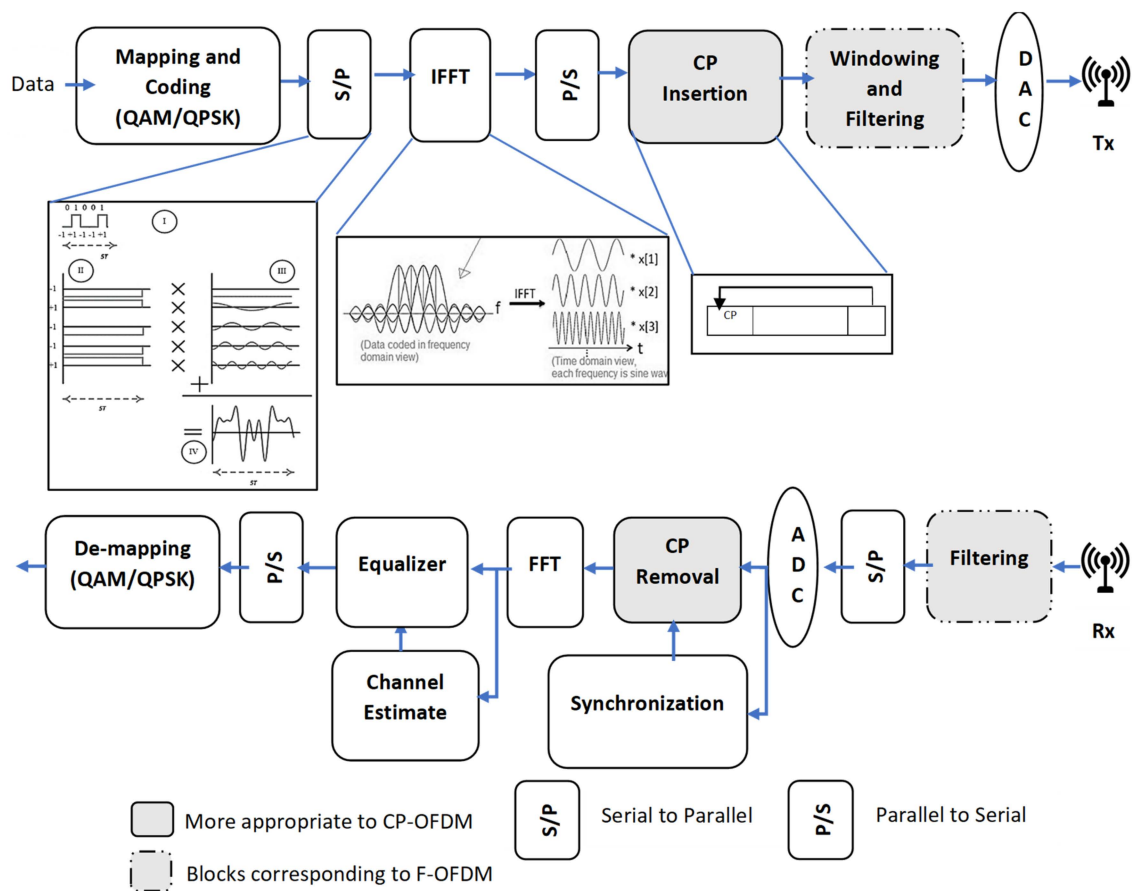
Figure 7. OFDM transceiver: firstly, the serial to parallel (S/P) converter splits the given data to several parallel streams which are converted to symbols through the mapping block. Secondly, the output of the IFFT block, after parallel to serial (P/S) conversion, is given to the next block for insertion of the CP. After the spectrum shaping process, the data are converted to analogue signals to be transmitted through the Tx antenna. In the receiver side, other filtering and S/P conversion processes are performed, and the signal is converted to digital data (symbols). Afterwards, the CP needs to be removed from the symbols, and an FFT is performed. The channel estimation is the most important block in the receiver. The given output data of this block are given to the equalizer to correct the channel effect. Finally, after P/S conversion, the symbols are de-mapped to bits. The CP insertion and removal blocs are used with cyclic prefix OFDM (CP-OFDM), which widely reduces the ISIs.

Let us consider a symbol to transmit:

$$s^T = \begin{bmatrix} s_0 \ s_1 \ldots \ s_{L-1} \end{bmatrix} \tag{7}$$

L is the size of the symbol s.
Considering the CP, the symbol is presented by the next formula:

$$s^T = \begin{bmatrix} s_{L-L_g} \ldots s_{L-1} \ s_0 \ s_1 \ldots \ s_{L-1} \end{bmatrix} \tag{8}$$

L_g is the number of CP samples.
We assume that the channel is time invariant with N taps and an impulse response given by:

$$c^T = \begin{bmatrix} c_0 \ c_1 \ldots \ c_{N-1} \end{bmatrix} \tag{9}$$

For single-carrier systems, the received signal is obtained through a simple convolution of the channel impulse response with the initial symbol. Nevertheless, for CP-OFDM

systems, a circular convolution is performed. Therefore, the received signal y, considering $R < L_g$, will be expressed as:

$$
\begin{bmatrix} y_0 \\ y_1 \\ \vdots \\ \vdots \\ \vdots \\ y_{L-1} \end{bmatrix} = \begin{bmatrix} c_0 & 0 & \cdots & 0 & c_{N-1} & \cdots & c_1 \\ \vdots & \ddots & \ddots & & \ddots & \ddots & \vdots \\ \vdots & & \ddots & \ddots & & \ddots & c_{N-1} \\ c_{N-1} & & & \ddots & \ddots & & 0 \\ 0 & \ddots & & & \ddots & \ddots & \vdots \\ \vdots & \ddots & \ddots & & & \ddots & 0 \\ 0 & \cdots & 0 & c_{N-1} & \cdots & \cdots & c_0 \end{bmatrix} \begin{bmatrix} s_0 \\ \vdots \\ \vdots \\ \vdots \\ \vdots \\ s_{L-1} \end{bmatrix} + \eta = Fs + \eta \quad (10)
$$

η refers to the noise term related to the channel.

Otherwise, if $R > L_g$, some Inter-Symbol Interferences (ISIs) appear.

The matrix F can be diagonalized by Fourier transform:

$$
\begin{cases} F = E^{-1}DE \\ D = \begin{bmatrix} D_0 & 0 & \cdots & 0 \\ & D_1 & \cdots & 0 \\ \vdots & & \ddots & \vdots \\ 0 & \cdots & 0 & D_{N-1} \end{bmatrix} \end{cases} \quad (11)
$$

where E and E^{-1} are the FFT and IFFT matrices, respectively.

3.2.3. MIMO-OFDM Variants

There are five (principally four) OFDM variants tested within MIMO systems, as summarized in Table 4. The most important, drawing real improvement with MIMO technology, are CP-OFDM, UF-OFDM, GFDM, and F-OFDM. Nevertheless, CP-OFDM-WOLA is cited by several researchers as a good candidate to work with MIMO systems. Instead of using filters, as with the normal OFDM scheme, WOLA-OFDM uses extension and windowing techniques to reduce OOB emissions [88,89]. In addition, the classic FBMC technique has been announced as being incompatible with MIMO systems [84] as it makes the implementation of traditional coding and channel estimation algorithms very difficult. However, the MIMO FBMC-OQAM scheme has attracted a lot of researchers [90].

Table 4. MIMO-OFDM variants.

OFDM Variants		
CP-OFDM	Cyclic prefix OFDM	[91]
UF-OFDM or UFMC	Universal filtered OFDM or universal filtered multi-carrier	[83,91,92]
CP-OFDM-WOLA	Weighted overlap and add CP-OFDM	[88,89] [1]
GFDM	Generalized OFDM	[93,94]
F-OFDM	Filtered OFDM	[95]
FBMC	Filter-bank multi-carrier	[83,96]

[1] WOLA-OFDM was analyzed by several researchers as being a good candidate that will perform very well with MIMO systems, but to the best of our knowledge, there is no experimental study which proves it.

Figure 7 explains very clearly the additional blocks needed to implement CP-OFDM and F-OFDM as well. Nonetheless, a brief introduction to UF-OFDM, GFDM, and FBMC-OQAM is given in the following.

- GFDM

GFDM deploys a circular pulse shaping to diminish the inter-carrier interference (ICI) phenomena. In comparison with OFDM, GFDM is more flexible to carrier frequency offset and time synchronization-induced errors [97].

The baseband scheme of a MIMO-GFDM transceiver [94,97] is given in Figure 8.
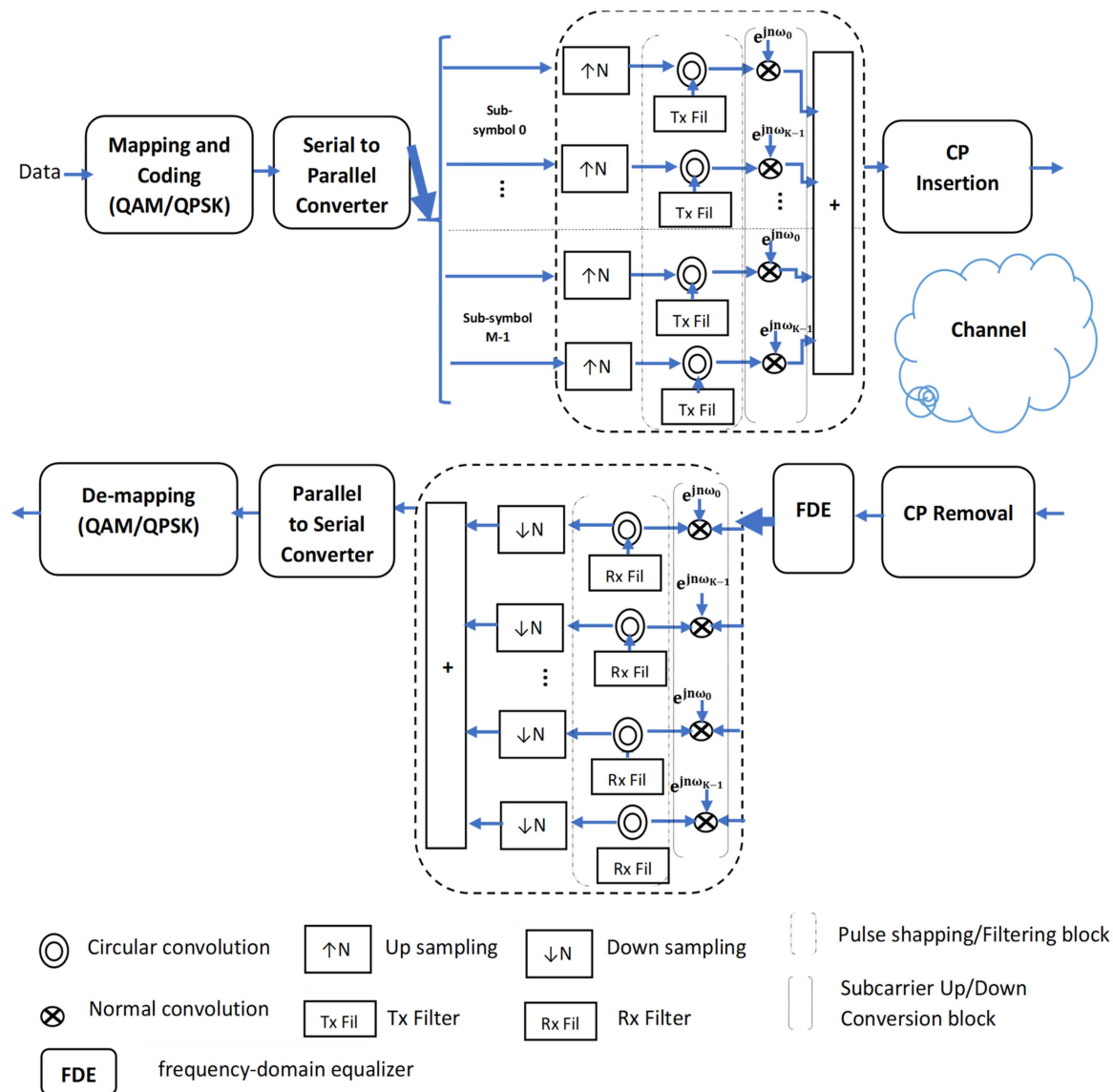
Figure 8. GFDM transceiver: the GFDM modulator consists of two stages, pulse shaping and subcarrier up-conversion. In the demodulator, those operations are inversed: subcarrier down-conversion and filtering.

The mapped symbols (with QAM, QPSK, or BPSK) are converted to parallel sub-streams for padding K subcarriers with M sub-symbols.

The parallel streams are up-sampled, with a sampling factor N, to correct the sub-symbol position in the block [97]. Afterwards, a circular convolution with a Tx filter is performed to exclude replicated samples; so, the subcarriers could be shifted to their center frequencies afterwards. Only one CP is inserted for all the concatenated M sub-symbols. In the receiver side, the CP is cut from the data, in addition to the other reversed operations performed to retrieve the final data. The equalization is for channel effect correction. The GFDM still suffers from a few drawbacks, especially a higher out-of-band (OOB) emission problem and high-complexity computation.

- UF-OFDM

UF-OFDM is a promising waveform which uses linear filters and eliminates the cyclic prefix. The baseband structure of the transceiver [97] is presented in Figure 9. The mapped symbols are converted to parallel streams. After computing an M-point IFFT over each sub-band, a band filter is applied. In fact, the use of the Dolph–Chebyshev bandpass filter (BPF) helps to tackle the OOB emissions [91,97]. Next, the filtered sub-bands are superposed and sent through the channel.
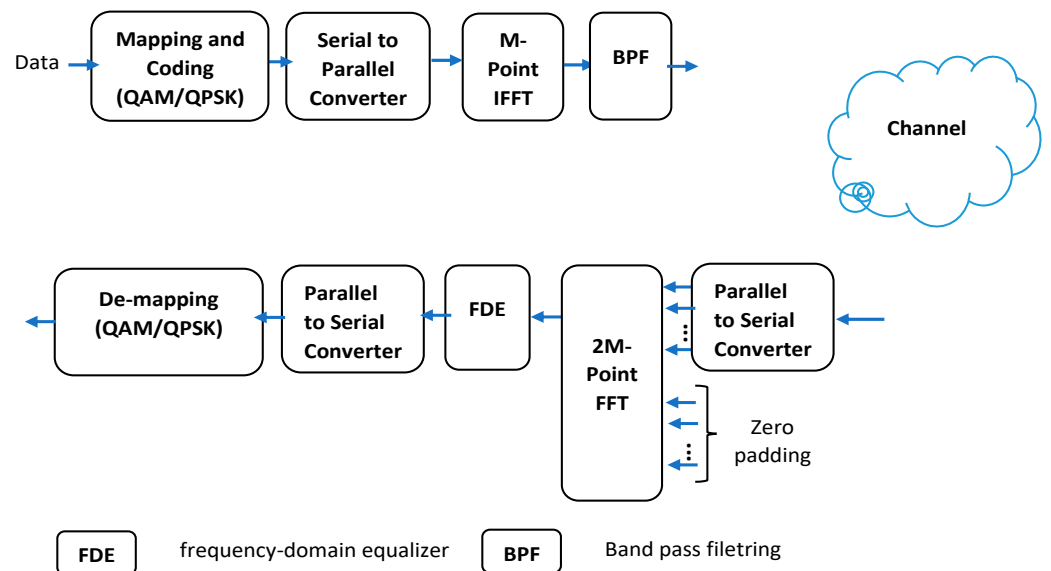
Figure 9. UF-OFDM transceiver.

A zero-padding process is performed from the receiver side. In fact, every symbol is padded with N − L zeros, where L is the BPF filter (in the transmitter side) length. Afterwards, the signals are demodulated by 2M-point FFT. The demodulated signals, excluding the padded zeros, are given to the equalizer to eliminate the channel distortions. Finally, the symbols are de-mapped to bits.

UF-OFDM outperforms OFDM in terms of ICI and ISI reduction, PAPR, and spectral efficiency.

- FBMC-OQAM

The original version of FBMC does not deploy any CP and uses a pulse-shaping filter. Therefore, it offers lower spectral sidelobes and computation latency, in addition to robustness to multipaths in high-loss environments.

FBMC-OQAM uses QAM mapping, with in-phase and quadrature components that are diphase in time by half the symbol period, and a well-designed pulse-shape filtering to satisfy the orthogonality propriety. Hence, the interferences between the adjacent bands do not affect the quality of transmission for this scheme. In fact, the received data do not suffer from either ISI or ICI due to the orthogonality condition imposed between the adjacent bands.

The diagram of an FBMC-OQAM baseband transceiver is depicted in Figure 10. $s_k(m)$ represents the transmitted symbol with the frequency and time indexes k and m, respectively. $x_k(2\,m)$ and $x_k(2\,m + 1)$ are gathered by calculating the real and imaginary components of the symbol resulting from the mapping stage, respectively. g(t) is the time response of the symmetrical pulse-shaping filter [90].
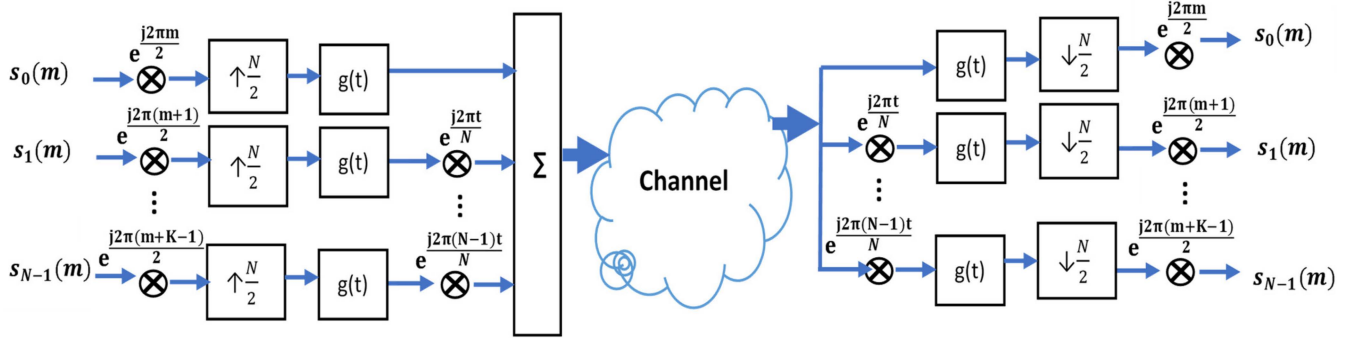
Figure 10. FBMC-OQAM transceiver.

3.2.4. MIMO-OFDM Variants Enhancement Studies

In addition to the existing OFDM waveform variants described before, several authors have suggested additional enhancements to those structures.

In this paragraph, we are going to give a brief insight into the most significant additions to the literature. Table 5 regroups those studies, with reference to the base waveform scheme.

Table 5. MIMO-OFDM variants enhanced schemes.

Enhancement of Study	OFDM	CP-OFDM	UFMC	GFDM	F-OFDM	FBMC
Chang and Ueng [98]				X		
Sharief and Sairam [99]	X					
Singh, et al. [100]			X			
Zakaria and Le Ruyet [101]						X
Zhao, et al. [102]						X
Yu, et al. [103]					X [1]	
Jin, et al. [104]						X
Aminjavaheri, et al. [105]		X				
Pereira, et al. [106]		X				

[1] It is theoretically proven that it is compatible with MIMO systems, but not tested experimentally.

Chang and Ueng [98] recommend a GFDM receiver scheme based on index modulation (IM) [107], considering a fading channel variable in time. The designed architecture (please refer to Figure 11) overcomes the defects introduced by shaping filters used with GFDM, namely self-created inter-carrier interference (ICI) and ISI as well. It deploys two-phase rotations to work for multipath transmission in fast-fading environments. The optimal phase rotations are obtained by maximizing the carrier-to-interference ratio (CIR). In fact, the authors suggested a new algorithm that uses the adaptive normalized block least-mean-squared (NBLMS) method [108], which allows the avoidance of the feedback of the carrier frequency offset. The Kalman algorithm was chosen to model the time variation of the channel using the pilot-symbol-aided estimation technique [109], combined with the turbo minimum mean square error (MMSE) equalizer [110]. In fact, the turbo equalizer deploys an iterative scheme to update the Kalman channel estimator, equalizer, and decoder blocks, given values until the convergence is achieved.

The log-likelihood ratio (LLR) is used to determine the current active carrier. It was proven that the current receiver scheme could reduce the decoding process for the current active subcarrier.

Sharief and Sairam [99] have suggested a new redundant discrete wavelet-based MIMO-OFDM (MIMO-RDWT-OFDM) framework, depicted in Figure 12. The utilization of the new introduced redundant discrete wavelet transform, which does not have the down-sampling step in the decomposition tree, widely improves the spectral efficiency of the transceiver, and it could be deployed in Additive White Gaussian Noise (AWGN) channels such as the Rayleigh fading model as it is more robust for noise [99].

Abbreviations

MRC Maximal Ratio Combining	**LLR** Log-Likelihood Ratio
Π denote the interleaver	**Π^{-1}** denote the de-interleaver
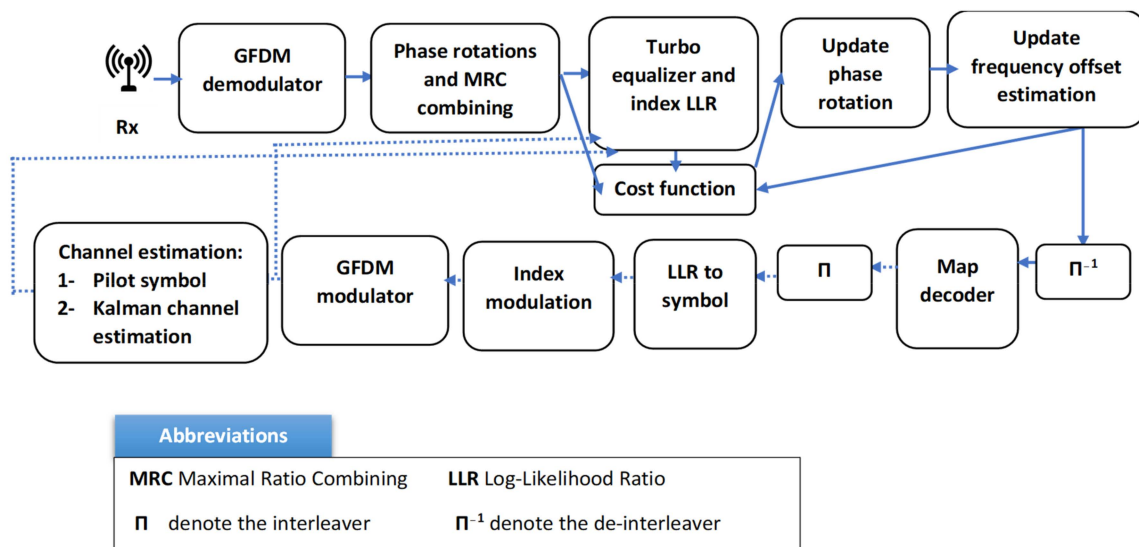
Figure 11. MIMO turbo GFDM-IM receiver: first, two-phase rotations are computed on initial carrier frequency offset values. Afterwards, the phase value for ICI interference correction is computed by an adaptive recommended NBLMS algorithm. The initial channel values are estimated by the pilot symbol. Accordingly, the LLR detector can localize the data position. Finally, there is the turbo equalization, where the mean and variance of the output signal are supplied to the developed Kalman channel estimation block to conduct calculations for the next iterations.
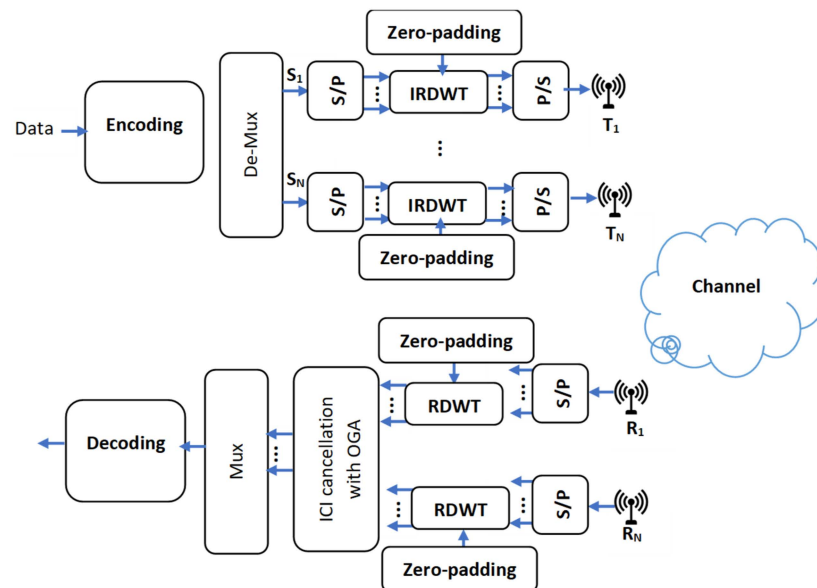
Figure 12. MIMO-RDWT-OFDM transceiver.

In addition, the MIMO-RDWT-OFDM model deploys an optimal genetic algorithm (OGA) to obtain optimized weights for the ICI cancellation scheme.

Singh, Naik and Kumar [100] have recommended a NOMA-UFMC-based Radio Access (NOMURA) downlink scheme (please refer to Figure 13) to enhance the throughput and system capacity. The base station groups the end users, following their Signal to Interference Noise Ratio (SINR), into two groups: Lower SINR Users (LSUs) and Higher SINR Users (HSUs). The LSU and HSU information is concatenated using superposition coding (SC) with a power ratio value of γ and $1 - \gamma$, respectively. SC is deployed with a Multiuser Superposition Transmission (MUST) Category 1 technique previously deployed in the 3GPP specifications [111], where HSU symbols are superimposed over LSUs with a

non-gray bit-mapping algorithm. Thereafter, UFMC is applied for every sub-band, with specific filtering parameters according to every user requirement.
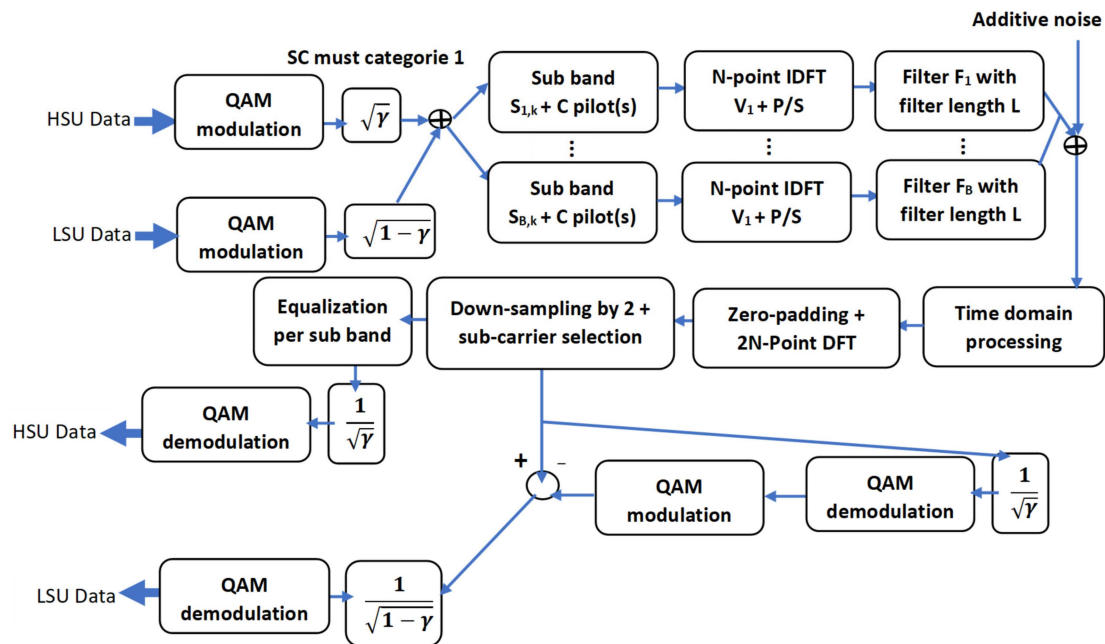
Figure 13. MIMO NOMORA system: P/S and S/P are abbreviations for parallel to serial and serial to parallel, respectively. F1, . . . , FB (this refers to the filter used for sub-band B) filter parameters depend on the users' requirements.

The recommended transceiver is tested under AWGN as well as Rayleigh fading environments. As described in Figure 13, the zero padding is performed to increase the length of the transmitted symbols to give them as input to the 2N-point discrete Fourier transform (DFT) block. A zero-forcing equalization was considered to correct the channel effect. In the demodulation part, LSUs threaten the HSU user signals as noise to extract the LSU original symbols. However, the HSU signals are reconstructed by demodulating and modulating the received signals to subsequently reconstruct the LSU signals, which are subtracted from the received signal to finally obtain the HSU data to be demodulated.

Zakaria and Le Ruyet [101] propose a new FFT-FBMC scheme with less interference terms in comparison to the original OFDM algorithm. The FFT-FBMC deploys DFT and CP insertion blocks (with a lower CP length), which make the scheme more complex but highly compatible with MIMO signal-processing algorithms. The transmission strategy uses guard intervals as well to isolate the adjacent subcarriers. The scheme was tested with maximum likelihood detection and Alamouti space–time coding algorithms.

Zhao, Gong and Schellmann [102] have introduced a novel FBMC-OQAM scheme to minimize inter-block interference by performing a single-band (SSB) filtering on the edge subcarriers of the resource blocks. This filtering procedure helps to preserve the orthogonality between the sub-symbols within the same block and allows the transceiver to reach the complex field orthogonality at the edges without the need to insert any guard intervals. In this context, a novel resource mapping scheme was chosen, which is shown in Figure 14. This scheme allocates Sc 0 (referring to the SSB filtered edge carrier) as well to the two initial resources in an alternating way.
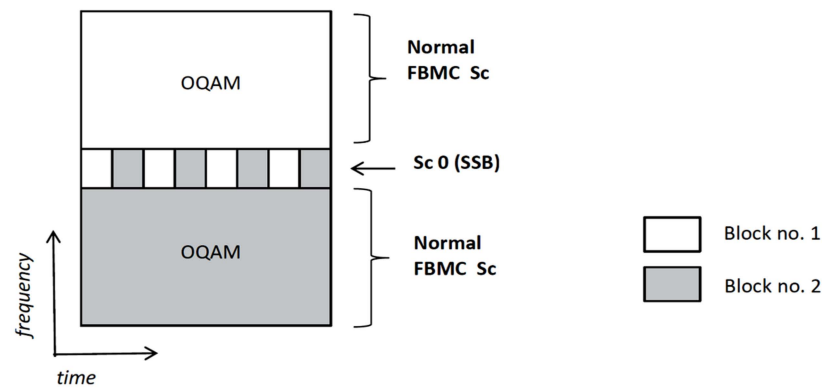
Figure 14. The resource mapping scheme.

Another enhanced FBMC based waveform, proposed by Jin, Hu, Huang, Li, Zhang and Ma [104], introduces a new conjugated FBMC-OQAM scheme. The authors take advantage of the fact that the pulse-shaping filter of the FBMC-OQAM systems exhibits odd symmetry, and the interferences that destruct the orthogonality (the intrinsic inter-symbol and the inter-carrier interferences) are strictly related to the neighboring symbols. Therefore, the idea was to divide the time-frequency resources into two parts, allowing the transmission of the original symbols and the corresponding conjugated version of the original ones. A unique signal-processing procedure is used to combine two conveniently separated sub-blocks. The recommended FBMC-OQAM system achieves an optimizing diversity gain.

Yu, Guanghui, Xiao, Zhen, Jun and Bo [103] were among the multiple other authors that theoretically proved that the filter bank OFDM (FB-OFDM) was compatible with MIMO systems. The baseband diagram of the transceiver is presented in Figure 15. The main difference between this scheme and the one of the traditional OFDM technique is the filtering part.
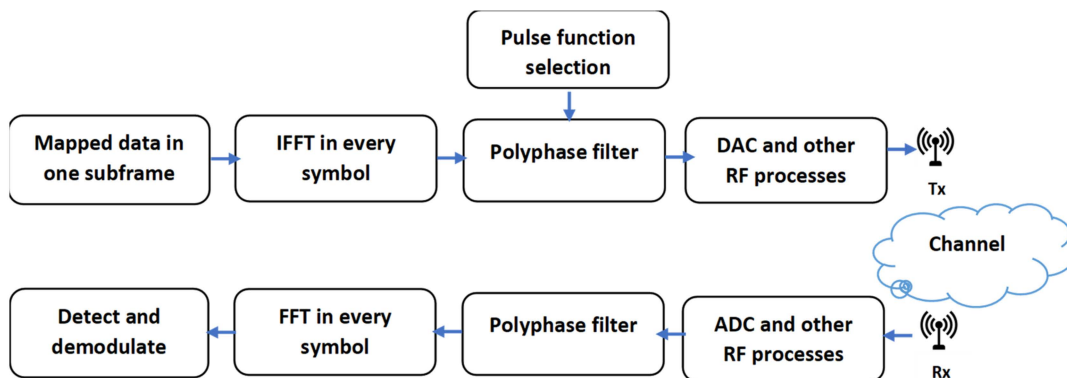
Figure 15. FB-OFDM transceiver.

Aminjavaheri, Farhang, Rezazadehreyhani, Doyle and Farhang-Boroujeny [105] proposed to remove the CP from the OFDM in massive MIMO systems. In addition, a time-reversal (TR) technique was used to resolve the saturation problems with the conventional frequency-domain-combining techniques: combining zero forcing and minimum mean square error detectors. The designated architecture achieves high spectral efficiency in realistic conditions.

Pereira, Bento, Gomes, Dinis and Silva [106] introduced the Time-Interleaved Block Windowed Burst-OFDM (TIBWB-OFDM) waveform technique, which is easily applied to MIMO, as presented in Figure 16. The idea was to cluster the data into windowed (with a time-square root-raised cosine filter) short OFDM blocks, zero padded (ZP). The small size FFTs and ZP integrated blocks widely improve the power efficiency and reduce the PAPR.
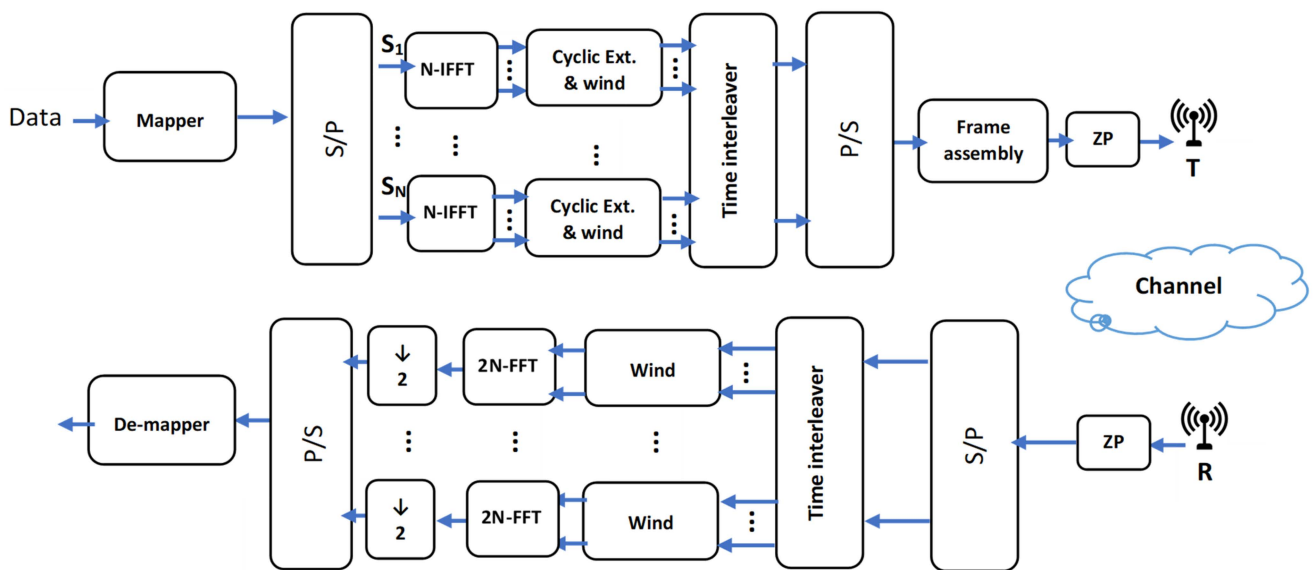
Figure 16. TIBWB-OFDM transceiver.

3.3. MIMO-OFDM Block Enhancements

In the literature, interesting studies were presented to enhance the MIMO-OFDM transceiver performance. Notably, the studies related to the channel estimation and equalization process. In the following, the relative studies and notions will be further expanded.

3.3.1. Channel Estimation

The MIMO-OFDM channel estimation schemes in the literature could fall under three main classes: pilot-aided (or training-based), blind techniques and semi-blind ones, and decision-directed channel estimation.

Quite a few innovative works have been found in the literature with regard to pilot-aided techniques, due to the induced processing overload of the pilots' data.

Table 6 gives a vision about the general classification of channel estimation for MIMO-OFDM wireless communication systems, in addition to the corresponding study references for every algorithm type. In the following, those studies will be more detailed in the proper context.

Table 6. MIMO-OFDM channel estimation algorithms classification.

Classification	Pilot-Aided (or Training-Based)	Blind [112] and Semi-Blind			Decision-Directed	
		Statistical Methods		Deterministic Methods	Hard	Soft
		2nd Order	High Order			
References	[113–124]	[125–127]	[128,129]	[130–133]	[134]	[135–139]

- Pilot-aided channel estimation algorithms

The pilot-assisted channel estimation or training-based technique inserts training pilots, which are well known by the receiver, to the transmitted sequence of symbols. Therefore, the receiver could extract CSI information, which is gathered by an interpolation between the different CSI values already extracted from the pilot sequences.

In fact, the pilots' arrangement could be in three types: comb type [113], block type [113,114], or 2D-grid type [118]. Figure 17 gives a better vision of the three situations.
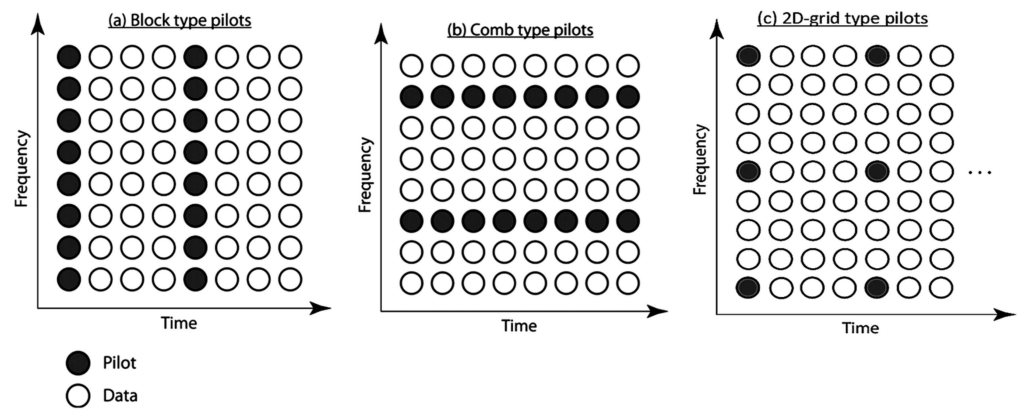
Figure 17. Pilot arrangement possible situations: (**a**) block type; (**b**) comb type; (**c**) 2D-grid type.

The shaded circles represent pilot symbols, whereas the unshaded ones represent the symbols to be transmitted. The horizontal axis is the time direction, and the vertical one is the frequency direction that represents the OFDM subcarriers.

The general scheme of a pilot-aided channel estimator (please refer to Figure 18) is composed of an LS/LMMSE estimator block, a frequency, and a time interpolator block, respectively, and a denoising and truncation block. The LS/LMMSE block calculates the channel frequency response using the received pilot symbols. The next step is to convert this response to the time domain. Afterwards, a denoising and truncation process is performed.
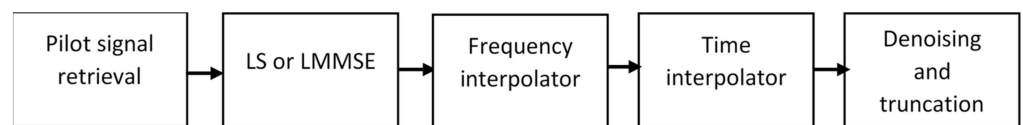
Figure 18. Pilot-based channel estimation scheme.

Some of the used frequency interpolators in the literature are: linear, second order, cubic spline, time domain-based, low-pass [140]; and DFT-based interpolators [117,118].

The block-type estimation is performed in the time domain, while for the comb type it is performed in the frequency domain.

The most adopted algorithms for channel estimation using the block-type pilot are: least squares [113,121,122] and Linearity Minimum Mean Squared Error (LMMSE) [139].

In [113], an LS channel estimator was investigated based on the block-type pilot structure and the comb-type pilot structure, with average MSE lower bounds.

In [114], a reduced-based LS estimator was designed, accepting the assumption that the channel was quasi-static over every two OFDM symbols, and their neighboring pilots were consecutively grouped as an equispaced cluster. The pilot is inserted into a designated block at each Tx antenna, i.e., it is sent periodically in the time domain. The channel response matrices are decoupled for every Tx antenna. Therefore, the MIMO channel estimation problem is formulated as a simple Single Input Output (SISO) corresponding channel estimator.

In [115], a channel estimator based on MMSE, which requires the calculation of the inverse of the channel autocorrelation matrix, was proposed. Hence, a singular value decomposition was used to reduce the induced complexity. The nominated comb-type pilot-based technique was used within a space–time block coding (STBC).

Conventionally, the comb-type pilot is the most used for the relatively small MIMO–OFDM architectures [116]. However, with more complex architectures, the amount of overhead increase and the choice of pilot sequence become a more important point when avoiding the pilot contamination problem (the case of using the same pilot sequence). Thus,

several authors [117,119] have opted to use the Zadoff Chu (or generalized Chirp-like) sequences, due to their orthogonality characteristics.

In [117], the estimation was performed using a DFT-based method in the time domain; the interpolation step was completely omitted. Zheng, Su and Wang [117] took advantage of the fact that a delay in the time domain is transposed as a phase shift in the frequency domain. Therefore, they inserted the pilots in the frequency domain, while the estimation was performed in the time domain.

In [118], a 2D grid-type scheme with a DFT-based time interpolator block was chosen for a massive MIMO system, due to its lower complexity. The nominated block incorporates a 2-point DFT (instead of the N-point DFT in conventional algorithm) process to optimize the use of the storage resources. The algorithm was simulated in various Rayleigh fading channel conditions with the universal threshold truncation technique [141].

Another training scheme where the pilots are spread in both time and frequency directions was designated in [119]. The novel time-frequency training OFDM scheme (TFT-OFDM) performs, jointly, a time estimation and an N-point DFT-based frequency estimation. The two estimators are unified under the same framework.

However, in [120], the authors investigate a different pilot-symbol scheme which adopts an ML estimator followed by a Wiener filtering approach for an LTE MIMO-OFDM system. The conducted study proved that a denser pilot combined with a partial knowledge of some statistics of the channel could attenuate the BER affected by interpolation error accumulation.

Hlaing, Al-Dhahir and Yinghui [121] consider a robust least-squares estimation for a channel with frequency offset and phase noise, while Hardjawana, Li, Vucetic, Li and Yang [122] choose a novel receiver structure based on pilot symbols and an iterative soft-estimate. In [122], the estimator is based on an LS time-domain interpolator. The soft estimate was realized through an improved maximum a posteriori (MAP) decoder.

Despite the traditional LS- and LMMSE-based estimators that have a relatively limited performance with the existence of strong interferences, novel innovative approaches based on machine learning are being introduced [123,124,142].

A sparse Bayesian learning-based estimator was designated in an orthogonal space–time block coded MIMO-OFDM system for an approximatively sparse channel type [123]. This technique updates the channel coefficients within a maximization formulation based on an ML algorithm for the estimation of the hyper parameters of the channel. Moreover, in [124] a pilot selection idea was implemented using a cat swarm optimization to enhance the channel estimation process.

More recently, the need to provide full secrecy in sensitive data applications has spurred research in physical layer secure communications. The usage of MIMO by increasing the number of parallel and independent channels in a rich scattering environment has been recognized to be a tool to increase the uncertainty about the channel and therefore increase the equivocation rate at an illegitimate receiver (e.g., [143,144] and references therein).

- Blind and semi-blind channel estimation algorithms

The blind channel estimation algorithms rely on statistical proprieties, do not need prior knowledge about the transmitted signal, and do not require inserting pilots or training symbols at the transmitter level, thus allowing the sending of more data and the attainment of higher spectral efficiency. However, the semi-blind techniques use a part of the knowledge of the signal in addition to some statistical characteristics. Under this category, there are two sub-categories: statistical methods and deterministic techniques.

For statistical techniques, the cyclic statistic properties of the signals are requested in the receiver side, although the deterministic techniques need both the coefficients and the received signal for estimating the channel matrix.

The statistical techniques are second- [125–127] or higher-order statistics (HOS) [128,129].

In [125], a blind scheme for a zero-padding MIMO-OFDM system, based on the covariance statistics, was presented. The channel matrix was obtained by resolving an equation series resulting from the covariance matrix of the received signal by exploiting the

block Toeplitz structure. The linear equations were reformulated into a set of decoupled groups. Then, the channel matrix was calculated within an eigen-decomposition of the outer product matrix.

In [126], a semi-blind scheme based on circular precoding was suggested, where the autocorrelation matrix of the received data engenders a set of mathematical equations in relation with the outer product of the channel matrix and the coefficients induced by the precoder. Some information about channel matrices was extracted from those equations, thus a Hermitian matrix was created within it. The corresponding positive eigenvalues and eigenvectors of this Hermitian matrix allow, finally, the gathering of the channel matrix.

However, Wan, Zhu and Swamy [127] tested an idea to cancel the signal perturbation of the second-order statistics estimators. First, it was necessary to analyze the correlation matrix of the received data. Afterwards, a novel way to transmit the data, considering the perturbation that could be cancelled, was applied. Moreover, the authors proved that by using a few specific additional slots the performance of this technique could achieve an ideal case.

In [128], a blind iterative hybrid independent component analysis (HICA) estimation schema is presented. Initially, the authors apply the pulse-shaping method with a square root-raised cosine filter to reduce the ISIs. Next, the signals in the receiver are identified by determining the separation matrix. The estimated signal order is different for every HICA iteration because the algorithm is randomly initialized. Hence, only the information that will appear repetitively in every iteration will be significant. The estimated desired signal is selected based on HOS from common signals resulting from different iterations of the HICA algorithm. Despite this, Peken, Vanhoy and Bose [129] introduced another less complex adaptive independent component analysis-based scheme, applied to massive MIMO. The algorithm is an improvement of the work carried out in [145].

To resume, the performance of statistical algorithms is usually influenced by the finite data effect. The deterministic algorithms [130–133,139,146] are the more complex ones, but they converge faster.

In [130], a compressed sensing-based algorithm was suggested, where only a deterministic subset of the index is selected to place the pilots in the data to be transmitted. Hence, this leads to some new measurement matrices and a new reconstruction algorithm.

However, in [131] a space-alternating generalized expectation-maximization (SAGE)-related scheme for STBC is divulged. The channel coefficients are estimated at pilot positions by a decomposition of the superimposed received signals, while the rest of the coefficients are calculated by Wiener interpolation. In [132], it is another semi-blind SAGE-based algorithm that contributes to a periodic update of the pilot-related MMSE estimate. Conventional estimators request the insertion of more pilots and more knowledge about large-scale fading coefficients to attain the desired performance, while this algorithm deploys the data symbols to estimate the missing information.

The framework exposed in [133] is a special case for channels with faster time-varying characteristics. It is an optimized semi-blind sparse estimator with a cost function estimated by an enhanced differential evolution algorithm. The semi-blind estimation was performed by LMMSE and LS. Afterwards, the enhanced differential evolution algorithm was adopted to diminish the cost function and further optimize the estimator.

- Decision-directed channel estimation algorithms

For these techniques, the detected symbols are deployed in addition to relatively few pilots for estimating the channel. This kind of scheme gives more reliable results than the pilot-assisted techniques because there are no transmission errors. The decision-directed techniques first necessitate an initial estimation of the channel transfer function, calculated staring from the current received and detected data. This estimation is used afterwards as an a priori channel estimate during the treatment of the next symbols of the incoming time slot.

Those techniques are in two groups: soft and hard decision-directed methods.

In [134], a joint pilot-aided and hard blind decision-directed channel estimation (PA-DDCE) scheme is explained. The authors gather the initial channel estimate using the conventional LS algorithm. Then, this estimate is deployed to detect the next data symbol situated between any two adjacent pilot sub-carriers. Subsequently, those symbols become like additional pilot symbols that are used to complete the estimation of the missing channel coefficients on the frequency band.

However, Park, Choi, Lee and Shim [135], Park, Shim and Choi [136] have a soft decision-directed strategy, drawing an interesting performance, which uses an iterative detector and decoder to optimize the estimation process. The algorithm (partially demonstrated in Figure 19) utilizes virtual pilots as well as pilots for the channel re-estimation. In the beginning, posteriori LLRs are built by an addition of the extrinsic LLRs resulting from the MIMO detector and the prior LLRs resulting from the decoder.
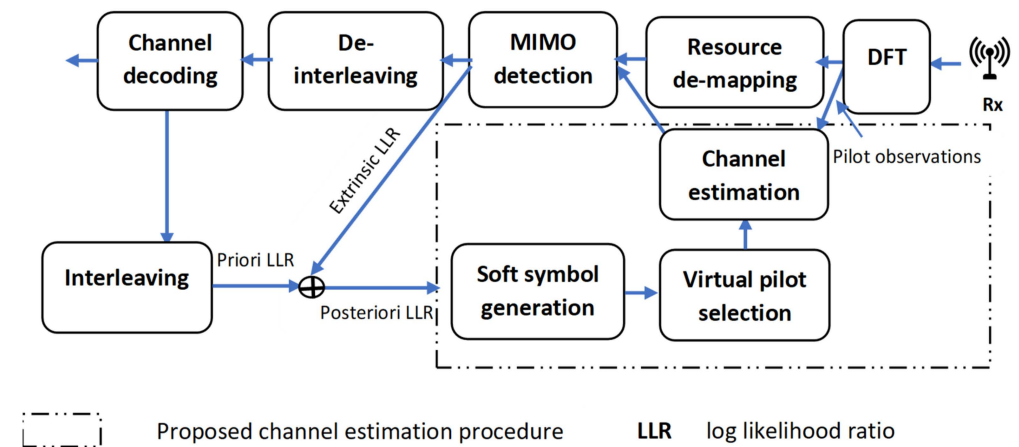
Figure 19. Channel iterative estimation scheme.

Thus, those posteriori LLRs are translated to soft symbols. Afterwards, virtual pilots are selected from the data available in the current window. In fact, the virtual pilot signals need to meet two principal conditions:

First, the magnitude of the posteriori LLRs needs to be high.

Second, the channels for the virtual pilots and the pilots need to be highly correlated.

However, after gathering those virtual pilots, the channel is re-estimated within the original pilots. The new estimate is given to the MIMO detection block in the next iteration.

In [137], a Kalman-like estimator based on a specific pipelined turbo equalizer logic was verified (please refer to [137] for further details about the architecture). Before forwarding the data to the Kalman estimator block, a specific algorithm was used to diminish the decision error correlation between the different pipeline stages.

Nonetheless, in [138], there is a deep neural network-based approach for the channel estimation of an STBC MIMO system. Two networks are trained to estimate the real and the imaginary part of the matrix of the fast-varying fading channel.

Finally, in [139], the performances of the LS, MMSE, and SAGE algorithms for a decision-directed estimator are assessed. The performance is improved by substituting some of the pilots with data symbols; then, the SAGE technique is used to downslide the loss induced.

3.3.2. Equalization

There are several logics to categorize the equalization algorithms. There are linear and non-linear equalizers. The linear algorithms are less complex than the non-linear ones, but they do not take into consideration the additive noise. Zero-forcing (ZF) [147], MMSE [148], and Least Mean Square (LMS) are all linear equalizers. The decision feedback equalizer (DFE) is a nonlinear equalizer that reduces ICI by an adopted filtering technique. We propose to categorize the existing algorithms as follows:

Type 1: Basic equalization techniques: ZP-, MMSE-, and LMS-based algorithms.

Type 2: Specialized techniques to reduce interference: turbo equalization [137,149], widely used to mitigate interference, is a technique that considers the channel as convolutional code and uses turbo decoding algorithms.

Type 3: Blind frequency-domain equalization: deploys a blind channel estimator.

A variety of proposed equalization algorithms for MIMO-OFDM systems are classified in Table 7. Every algorithm is related to its corresponding type, and it is attached with a little description.

Table 7. MIMO-OFDM equalization algorithm classification.

Type	References	Year	Main Idea	Key Algorithms
Type 1	[150]	2019	A symmetric successive over-relaxation (SSOR) method to reduce the complexity of the classical ZF precoding which uses the channel property of asymptotical orthogonality to compute the optimal relaxation parameters.	SSOR technique for ZF
Type 3	[151]	2019	- A supervised learning architecture to predict the constellation points based on pilot signals which constitue training data. - A new activation function was proposed to be able to use the famous stochastic gradient descent algorithm for optimization.	Deep neural network with gradient descent algorithm
Type 2	[149]	2019	- The Kalman channel estimation and turbo MMSE equalization are used. - The iterative algorithm repeats the channel estimation, equalization, and decoding operations until convergence. The feedback information received from the decoder is injected another time into the equalisation process.	Turbo MMSE equalizer with MAP decoder
Type 1	[148]	2018	Testing MMSE equalizer with a decision-directed channel estimator in a multipath fading channel	MMSE algorithm
Type 2	[152]	2012	Iterative receiver based on equal gain combining (EGC) and maximum ratio combining (MRC)	RGC, MRC and LLR
Type 3	[147]	2009	An independent component analysis-based equalizer: First the received signal is whitened by principal component analysis, using JADE to gather uncorrelated signals. A phase shifting is performed as well as a reordering technique.	JADE batch algorithm
Type 1	[147]	2009	Exchanging the order of the processing block: interpolation and the ZF equalizer stage. This operation is performed at each pilot position, then the ZF equalizer is interpolated over the whole grid.	ZF equalization
Type 2	[153]	2009	The oblique projection (OB) with QR-based factorization is used to separate the noise from the data. Afterwards, the resulting matrix is forwarded to the DFE equalizer.	DFE equalizer, associated with the OB
Type 3	[154]	2008	A semi-blind time domain equalization, using second-order statistics and a one-tape equalizer.	
Type 2	[155]	2007	a DFE equalizer combined with Recursive Least Squares (RLS) to compute the coefficient of the adaptive filter.	RLS algorithm
Type 1	[156]	2007	An MMSE equalizer based on QR factorization implemented on FPGA to compute the inverse of the filter matrix.	MMSE and QR factorization

4. Conclusions

The combination of MIMO transmission techniques with the OFDM waveform has brought an emerging technology to the wireless telecommunication field. In the last decade, MIMO-OFDM has drawn distinguished advances in terms of hardware and software innovations. Universities and telecommunication leaders have made prominent massive MIMO architectures operational and accessible for research proposals to further encourage new additions to the current literature.

We presented an extensive review of MIMO-OFDM, tackling several difficulties to regroup all the important research axes. The most important and recent references were included to point out the necessary information for the readers without redundancy. Nonetheless, some recent papers could have been missed as we mainly limited the resources to three databases: ISI Web of Science, IEEE Xplore, and Google Scholar. Hence, some papers were automatically excluded from the search, but the papers indexed on those databases have more impact on and relevance to the addressed topic. The reported state of the art concerned three essential points: MIMO hardware/software technology, MIMO waveforms, and MIMO-OFDM channel estimation and equalization.

From the above extensive search, some points can be noticed:

- The part on implementation is more limited to research testbeds that apply traditional channel estimation algorithms.
- The most deployed channel estimation algorithms are complex and have a lower level of mitigation of ICI.
- The equalization algorithms are quite limited in terms of performance.

In the next section, some challenges and research opportunities are highlighted.

4.1. Challenges

The most challenging problem in the MIMO-OFDM system is the elimination of the ICI and ISI interferences. One cumbersome solution would be to use a CP-OFDM variant. Nonetheless, with massive MIMO architecture and with some complex signal processing algorithms (channel estimation, equalization, coding, decoding) the process would cause a lot of latency, which would alter the communication with a lot of delays and errors. In fact, when the CP length is less than the channel impulse response, ISI and ICI degrade the performance of the receiver. The inherent idea is to choose a suitable channel estimator and a key equalization technique to fade away the interference effect.

4.2. Opportunities

There are some worthy ideas that could be exploitable for future research:

- The machine learning algorithm, as well as the empirical mode decomposition-based methods, draws interesting results for the channel estimating problem.
- The equalization techniques based on the wavelet decomposition technique are interesting.
- OFDM waveform enhanced schema.

Author Contributions: Conceptualization, P.M., A.G. and F.G.; methodology, H.H.; software, H.H.; validation, P.M., A.G. and F.G.; formal analysis, H.H.; investigation, H.H.; resources, P.M. and A.G.; data curation, H.H.; writing—original draft preparation, H.H. and H.F.T.A.; writing—review and editing, H.H., P.M., A.G. and H.F.T.A.; visualization, H.H., P.M. and A.G.; supervision, P.M. and A.G.; project administration, P.M.; funding acquisition, P.M. All authors have read and agreed to the published version of the manuscript.

Funding: This work was partially supported by the European Regional Development Fund (FEDER), through the Regional Operational Programme of Centre (CENTRO 2020) of the Portugal 2020 framework, through projects SOCA (CENTRO-01-0145-FEDER-000010) and ORCIP (CENTRO-01-0145-FEDER-022141). Fernando P. Guiomar acknowledges a fellowship from "la Caixa" Foundation (ID 100010434), code LCF/BQ/PR20/11770015. Houda Harkat acknowledges the financial support of the Programmatic Financing of the CTS R&D Unit (UIDP/00066/2020).

Institutional Review Board Statement: Not applicable.

Informed Consent Statement: Not applicable.

Data Availability Statement: Not applicable.

Acknowledgments: We would like to thank the editor and the reviewers for their comments which helped us improve the paper.

Conflicts of Interest: The authors declare no conflict of interest.

References

1. García-Naya, J.A.; González-López, M.; Castedo, L. An overview of MIMO testbed technology. In Proceedings of the 4th International Symposium on Image and Video Communications over Fixed and Mobile Networks (ISIVC'08), Bilbao, Spain, 9–11 July 2008.

2. Delson, T.R.; Jose, I. A Survey on 5G Standards, Specifications and Massive MIMO Testbed Including Transceiver Design Models Using QAM Modulation Schemes. In Proceedings of the 2019 International Conference on Data Science and Communication (IconDSC), Bangalore, India, 1–2 March 2019; IEEE: Piscataway, NJ, USA, 2019; pp. 1–7.

3. Shafi, M.; Molisch, A.F.; Smith, P.J.; Haustein, T.; Zhu, P.; Silva, P.D.; Tufvesson, F.; Benjebbour, A.; Wunder, G. 5G: A Tutorial Overview of Standards, Trials, Challenges, Deployment, and Practice. *IEEE J. Sel. Areas Commun.* **2017**, *35*, 1201–1221. [CrossRef]

4. Banelli, P.; Buzzi, S.; Colavolpe, G.; Modenini, A.; Rusek, F.; Ugolini, A. Modulation Formats and Waveforms for 5G Networks: Who Will Be the Heir of OFDM?: An overview of alternative modulation schemes for improved spectral efficiency. *IEEE Signal Process. Mag.* **2014**, *31*, 80–93. [CrossRef]

5. Wang, C.; Haider, F.; Gao, X.; You, X.; Yang, Y.; Yuan, D.; Aggoune, H.M.; Haas, H.; Fletcher, S.; Hepsaydir, E. Cellular architecture and key technologies for 5G wireless communication networks. *IEEE Commun. Mag.* **2014**, *52*, 122–130. [CrossRef]

6. Amin, M.R.; Trapasiya, S.D. Space Time Coding Scheme for MIMO system-Literature Survey. *Procedia Eng.* **2012**, *38*, 3509–3517. [CrossRef]

7. Chen, S.; Zhang, J.; Zhang, J.; Björnson, E.; Ai, B. A survey on user-centric cell-free massive MIMO systems. *Digit. Commun. Netw.* **2021**, *in press*. [CrossRef]

8. Mokhtari, Z.; Sabbaghian, M.; Dinis, R. A Survey on Massive MIMO Systems in Presence of Channel and Hardware Impairments. *Sensors* **2019**, *19*, 164. [CrossRef]

9. Ijiga, O.E.; Ogundile, O.O.; Familua, A.D.; Versfeld, D.J. Review of channel estimation for candidate waveforms of next generation networks. *Electronics* **2019**, *8*, 956. [CrossRef]

10. Wen, F.; Wymeersch, H.; Peng, B.; Tay, W.P.; So, H.C.; Yang, D. A survey on 5G massive MIMO localization. *Digit. Signal Process.* **2019**, *94*, 21–28. [CrossRef]

11. Zheng, K.; Zhao, L.; Mei, J.; Shao, B.; Xiang, W.; Hanzo, L. Survey of Large-Scale MIMO Systems. *IEEE Commun. Surv. Tutor.* **2015**, *17*, 1738–1760. [CrossRef]

12. Yang, S.; Hanzo, L. Fifty Years of MIMO Detection: The Road to Large-Scale MIMOs. *IEEE Commun. Surv. Tutor.* **2015**, *17*, 1941–1988. [CrossRef]

13. Paul, B.S.; Bhattacharjee, R. MIMO channel modeling: A review. *IETE Tech. Rev.* **2008**, *25*, 315–319. [CrossRef]

14. Yu, K.; Ottersten, B. Models for MIMO propagation channels: A review. *Wirel. Commun. Mob. Comput.* **2002**, *2*, 653–666. [CrossRef]

15. Fatema, N.; Hua, G.; Xiang, Y.; Peng, D.; Natgunanathan, I. Massive MIMO Linear Precoding: A Survey. *IEEE Syst. J.* **2018**, *12*, 3920–3931. [CrossRef]

16. Qiao, G.; Babar, Z.; Ma, L.; Ahmed, N. Channel Estimation and Equalization of Underwater Acoustic MIMO-OFDM Systems: A Review Estimation du canal et l'égalisation des systèmes MEMS-MROF acoustiques sous-marins: Une revue. *Can. J. Electr. Comput. Eng.* **2019**, *42*, 199–208. [CrossRef]

17. Fette, B. Introducing Adaptive, Aware, and Cognitive Radios. In *Cognitive Radio, Software Defined Radio, and Adaptive Wireless Systems*; Arslan, H., Ed.; Springer: Dordrecht, The Netherlands, 2007; pp. 1–16.

18. Luther, E. 5G massive MIMO testbed: From theory to reality. White Paper. 2014. Available online: https://www.ni.com/en-rs/innovations/white-papers/14/5g-massive-mimo-testbed--from-theory-to-reality--.html (accessed on 4 May 2022).

19. Hasan, W.B.; Harris, P.; Doufexi, A.; Beach, M. Real-Time Maximum Spectral Efficiency for Massive MIMO and its Limits. *IEEE Access* **2018**, *6*, 46122–46133. [CrossRef]

20. Zhang, C.; Qiu, R.C. Massive MIMO testbed-implementation and initial results in system model validation. *arXiv* **2014**, arXiv:1501.00035.

21. Ryan, Ø.; Debbah, M. Random Vandermonde matrices-part I: Fundamental results. *IEEE Trans. Inf. Theory* **2008**, *1*, 1–20.

22. Ryan, Ø.; Debbah, M. Random vandermonde matrices-part ii: Applications. *IEEE Trans. Inf. Theory* **2008**, *1*, 1–13.

23. Vieira, J.; Malkowsky, S.; Nieman, K.; Miers, Z.; Kundargi, N.; Liu, L.; Wong, I.; Öwall, V.; Edfors, O.; Tufvesson, F. A flexible 100-antenna testbed for Massive MIMO. In Proceedings of the 2014 IEEE Globecom Workshops (GC Wkshps), Austin, TX, USA, 8–12 December 2014; IEEE: Piscataway, NJ, USA, 2014; pp. 287–293.

24. Edfors, O. LuMaMi-A Flexible Testbed for Massive MIMO. Available online: https://people.kth.se/~{}perz/ewtbwr/2014/abstracts/Edfors.pdf (accessed on 1 March 2022).

25. Jiang, X.; Kaltenberger, F. Demo: An LTE compatible massive MIMO testbed based on OpenAirInterface. In Proceedings of the WSA 2017, 21th International ITG Workshop on Smart Antennas, Berlin, Germany, 15–17 March 2017; IEEE: Piscataway, NJ, USA, 2017; pp. 1–2.

26. Malkowsky, S.; Vieira, J.; Liu, L.; Harris, P.; Nieman, K.; Kundargi, N.; Wong, I.C.; Tufvesson, F.; Öwall, V.; Edfors, O. The World's First Real-Time Testbed for Massive MIMO: Design, Implementation, and Validation. *IEEE Access* **2017**, *5*, 9073–9088. [CrossRef]

27. Batra, A.; Wiemeler, M.; Kreul, T.; Goehringer, D.; Kaiser, T. A Massive MIMO Signal Processing Architecture for GHz to THz Frequencies. In Proceedings of the 2018 First International Workshop on Mobile Terahertz Systems (IWMTS), Duisburg, Germany, 2–4 July 2018; IEEE: Piscataway, NJ, USA, 2018; pp. 1–6.

28. Zamfirescu, C.; Vulpe, A.; Halunga, S.; Fratu, O. Spatial Multiplexing MIMO 5G-SDR Open Testbed Implementation. In Proceedings of the International Conference on Future Access Enablers of Ubiquitous and Intelligent Infrastructures, Sofia, Bulgaria, 28–29 March 2019; pp. 197–213.

29. Ribeiro, C.; Gameiro, A. A software-defined radio FPGA implementation of OFDM-based PHY transceiver for 5G. *Analog. Integr. Circuits Signal Process.* **2017**, *91*, 343–351. [CrossRef]

30. Vielva, L.; Vía, J.; Gutiérrez, J.; González, Ó.; Ibáñez, J.; Santamaría, I. Building a web platform for learning advanced digital communications using a MIMO testbed. In Proceedings of the 2010 IEEE International Conference on Acoustics, Speech and Signal Processing, Dallas, TX, USA, 14–19 March 2010; IEEE: Piscataway, NJ, USA, 2010; pp. 2942–2945.

31. Naya, J. Testbed Design for Wireless Communications Systems Assessment. Ph.D. Thesis, Universidade Da Coruna, A Coruña, Spain, 2010.

32. Bates, D.; Henriksen, S.; Ninness, B.; Weller, S.R. A 4×4 FPGA-based wireless testbed for LTE applications. In Proceedings of the 2008 IEEE 19th International Symposium on Personal, Indoor and Mobile Radio Communications, Cannes, France, 15–18 September 2008; pp. 1–5.

33. Nieto, X.; Ventura, L.M.; Mollfulleda, A. GEDOMIS: A broadband wireless MIMO-OFDM testbed, design and implementation. In Proceedings of the 2nd International Conference on Testbeds and Research Infrastructures for the Development of Networks and Communities (TRIDENTCOM 2006), Barcelona, Spain, 1–3 March 2006; pp. 10–121.

34. Ramirez, D.; Santamaria, I.; Pérez, J.; Via, J.; Tazón, A.; Garcia-Naya, J.; Fernández-Caramés, T.; López, M.G.; Perez-Iglesias, H.; Castedo, L. A flexible testbed for the rapid prototyping of MIMO baseband modules. In Proceedings of the 2006 3rd International Symposium on Wireless Communication Systems, Valencia, Spain, 6–8 September 2006; pp. 776–780.

35. Caban, S.; Mehlführer, C.; Langwieser, R.; Scholtz, A.L.; Rupp, M. Vienna MIMO testbed. *EURASIP J. Adv. Signal Process.* **2006**, *2006*, 054868. [CrossRef]

36. Sundance Multiprocessor Technology, SMT 365. Available online: https://www.sundance.com/product-range/sundance-products/archived-products/smt365-16-1/ (accessed on 1 March 2022).

37. Roy, S.; Bélanger, L. The design of an fpga-based mimo transceiver for wi-fi. *DSP Mag.* **2006**, *1*, 28–31.

38. Borkowski, D.; Brühl, L.; Degen, C.; Keusgen, W.; Alirezaei, G.; Geschewski, F.; Oikonomopoulos, C.; Rembold, B. SABA: A testbed for a real-time MIMO system. *EURASIP J. Appl. Signal Process.* **2006**, *2006*, 143. [CrossRef]

39. Dowle, J.; Kuo, S.H.; Mehrotra, K.; McLoughlin, I.V. An FPGA-based MIMO and space-time processing platform. *EURASIP J. Appl. Signal Process.* **2006**, *2006*, 1–14. [CrossRef]

40. Wilzeck, A.; El-Hadidy, M.; Cai, Q.; Amelingmeyer, M.; Kaiser, T. MIMO prototyping test-bed with off-the-shelf plug-in RF hardware. In Proceedings of the IEEE Workshop on Smart Antennas, Ulm, Germany, 13–14 March 2006.

41. Zhu, W.; Browne, D.; Fitz, M. An open access wideband multiantenna wireless testbed with remote control capability. In Proceedings of the First International Conference on Testbeds and Research Infrastructures for the DEvelopment of NeTworks and COMmunities, Trento, Italy, 23–25 February 2005; pp. 72–81.

42. Wallace, J.W.; Jeffs, B.D.; Jensen, M.A. A real-time multiple antenna element testbed for MIMO algorithm development and assessment. In Proceedings of the IEEE Antennas and Propagation Society Symposium, Monterey, CA, USA, 20–25 June 2004; pp. 1716–1719.

43. Lang, S.; Rao, M.; Daneshrad, B. Design and development of a 5.25 GHz software defined wireless OFDM communication platform. *IEEE Commun. Mag.* **2004**, *42*, S6–S12. [CrossRef]

44. Morawski, R.; Le-Ngoc, T.; Naeem, O. Wireless and wireline MIMO testbed. In Proceedings of the CCECE 2003-Canadian Conference on Electrical and Computer Engineering. Toward a Caring and Humane Technology (Cat. No. 03CH37436), Montreal, QC, Canada, 4–7 May 2003; pp. 1913–1916.

45. Murphy, P.; Lou, F.; Sabharwal, A.; Frantz, J.P. An FPGA based rapid prototyping platform for MIMO systems. In Proceedings of the The Thrity-Seventh Asilomar Conference on Signals, Systems & Computers, Pacific Grove, CA, USA, 9–12 November 2003; pp. 900–904.

46. Fabregas, A.G.; Guillaud, M.; Caire, G.; Gosse, K.; Rouquette, S.; Dias, A.R.; Bernardin, P.; Miet, X.; Conrat, J.-M.; Toutain, Y. A MIMO-OFDM testbed for wireless local area networks. In Proceedings of the Conference Record of the Thirty-Ninth Asilomar Conference onSignals, Systems and Computers, Pacific Grove, CA, USA, 30 October–2 November 2005; pp. 82–86.

47. Sezgin, I.C.; Dahlgren, M.; Eriksson, T.; Coldrey, M.; Larsson, C.; Gustavsson, J.; Fager, C. A Low-Complexity Distributed-MIMO Testbed Based on High-Speed Sigma–Delta-Over-Fiber. *IEEE Trans. Microw. Theory Tech.* **2019**, *67*, 2861–2872. [CrossRef]

48. Simeone, O.; Somekh, O.; Poor, H.V.; Shamai, S. Distributed MIMO Systems for Nomadic Applications Over a Symmetric Interference Channel. *IEEE Trans. Inf. Theory* **2009**, *55*, 5558–5574. [CrossRef]

49. Kun, Z.; Crisp, M.J.; Sailing, H.; Penty, R.V.; White, I.H. MIMO system capacity improvements using radio-over-fibre distributed antenna system technology. In Proceedings of the 2011 Optical Fiber Communication Conference and Exposition and the National Fiber Optic Engineers Conference, Los Angeles, CA, USA, 6–10 March 2011; IEEE: Piscataway, NJ, USA, 2011; pp. 1–3.

50. Gordon, G.S.D.; Crisp, M.J.; Penty, R.V.; White, I.H. Experimental Evaluation of Layout Designs for 3 × 3 MIMO-Enabled Radio-Over-Fiber Distributed Antenna Systems. *IEEE Trans. Veh. Technol.* **2014**, *63*, 643–653. [CrossRef]

51. Ahn, C.; Kim, J.; Ju, J.; Choi, J.; Choi, B.; Choi, S. Implementation of an SDR platform using GPU and its application to a 2 × 2 MIMO WiMAX system. *Analog. Integr. Circuits Signal Process.* **2011**, *69*, 107. [CrossRef]

52. Han, S.W.; Jin, Y.; Ahn, H.S.; Choi, S.W.; Hyeon, S.H. Implementation of an MU-MIMO system with GPU modem for non-codebook-based TDD LTE-A. In Proceedings of the The 18th IEEE International Symposium on Consumer Electronics (ISCE 2014), Jeju, Korea, 22–25 June 2014; IEEE: Piscataway, NJ, USA, 2014; pp. 1–2.

53. Roger, S.; Ramiro, C.; Gonzalez, A.; Almenar, V.; Vidal, A.M. Fully Parallel GPU Implementation of a Fixed-Complexity Soft-Output MIMO Detector. *IEEE Trans. Veh. Technol.* **2012**, *61*, 3796–3800. [CrossRef]

54. Wu, M.; Sun, Y.; Gupta, S.; Cavallaro, J.R. Implementation of a High Throughput Soft MIMO Detector on GPU. *J. Signal Process. Syst.* **2011**, *64*, 123–136. [CrossRef]

55. Gokalgandhi, B.; Segerholm, C.; Paul, N.; Seskar, I. Accelerating Channel Estimation and Demodulation of Uplink OFDM symbols for Large Scale Antenna Systems using GPU. In Proceedings of the 2019 International Conference on Computing, Networking and Communications (ICNC), Honolulu, HI, USA, 18–21 February 2019; IEEE: Piscataway, NJ, USA, 2019; pp. 955–959.

56. Caire, G.; Taricco, G.; Biglieri, E. Bit-interleaved coded modulation. *IEEE Trans. Inf. Theory* **1998**, *44*, 927–946. [CrossRef]

57. Raychaudhuri, D.; Seskar, I.; Ott, M.; Ganu, S.; Ramachandran, K.; Kremo, H.; Siracusa, R.; Liu, H.; Singh, M. Overview of the ORBIT radio grid testbed for evaluation of next-generation wireless network protocols. In Proceedings of the IEEE Wireless Communications and Networking Conference, Wuhan, China, 23–26 September 2005; pp. 1664–1669.

58. Bhagavatula, R.; Heath, R.W., Jr.; Linehan, K. Performance evaluation of MIMO base station antenna designs. *Antenna Syst. Technol. Mag.* **2008**, *11*, 14–17.

59. Li, Y.; Luo, Y.; Yang, G. High-Isolation 3.5 GHz Eight-Antenna MIMO Array Using Balanced Open-Slot Antenna Element for 5G Smartphones. *IEEE Trans. Antennas Propag.* **2019**, *67*, 3820–3830. [CrossRef]

60. Kamran Shereen, M.; Khattak, M.I.; Witjaksono, G. A brief review of frequency, radiation pattern, polarization, and compound reconfigurable antennas for 5G applications. *J. Comput. Electron.* **2019**, *18*, 1065–1102. [CrossRef]

61. Ojaroudi Parchin, N.; Jahanbakhsh Basherlou, H.; Al-Yasir, Y.I.; Abd-Alhameed, R.A.; Abdulkhaleq, A.M.; Noras, J.M. Recent developments of reconfigurable antennas for current and future wireless communication systems. *Electronics* **2019**, *8*, 128. [CrossRef]

62. Hussain, R.; Sharawi, M.S. A Cognitive Radio Reconfigurable MIMO and Sensing Antenna System. *IEEE Antennas Wirel. Propag. Lett.* **2015**, *14*, 257–260. [CrossRef]

63. Hussain, R.; Sharawi, M.S. Integrated reconfigurable multiple-input–multiple-output antenna system with an ultra-wideband sensing antenna for cognitive radio platforms. *IET Microw. Antennas Propag.* **2015**, *9*, 940–947. [CrossRef]

64. Kambali, V.; Abegaonkar, M.; Basu, A. Frequency reconfigurable compact MIMO antenna for WLAN application. In Proceedings of the 2017 International Symposium on Antennas and Propagation (ISAP), Phuket, Thailand, 30 October–2 November 2017; pp. 1–2.

65. Kotwalla, A.; Choukiker, Y.K. Design and analysis of microstrip antenna with frequency reconfigurable in MIMO environment. In Proceedings of the 2017 International conference of Electronics, Communication and Aerospace Technology (ICECA), Coimbatore, India, 20–22 April 2017; pp. 354–358.

66. Thao, H.T.P.; Luan, V.T.; Minh, N.C.; Journet, B.; Van Yem, V. A company frequency reconfigurable MIMO antenna with low mutual coupling for UMTS and LTE applications. In Proceedings of the 2017 International Conference on Advanced Technologies for Communications (ATC), Quy Nhon, Vietnam, 18–20 October 2017; pp. 174–179.

67. Duyen, T.H.; Pham, A.T. Performance analysis of mimo/fso systems using sc-qam signaling over atmospheric turbulence channels. *IEICE Trans. Fundam. Electron. Commun. Comput. Sci.* **2014**, *97*, 49–56. [CrossRef]

68. Cai, Q.; Wilzeck, A.; Kaiser, T. Evaluation of Synchronization andl Fractilonally Spaced Equalilzation in a MIMO SC-FDE Test-Bed. In Proceedings of the 2007 IEEE Radio and Wireless Symposium, Long Beach, CA, USA, 9–11 January 2007; pp. 527–530.

69. Wu, P.; Schober, R.; Bhargava, V.K. Optimal Tx-BF for MIMO SC-FDE Systems. *IEEE Commun. Lett.* **2013**, *17*, 1509–1512. [CrossRef]

70. Mokhtari, Z.; Sabbaghian, M.; Dinis, R. Massive MIMO downlink based on single carrier frequency domain processing. *IEEE Trans. Commun.* **2016**, *66*, 1164–1175. [CrossRef]

71. Nam, Y.-H.; Han, J.-K.; Zhang, J. Multiplexing of control and data in UL MIMO system based on SC-FDM. Patent No. CA2809325A, 1 March 2013.

72. Berardinelli, G.; de Temino, L.A.M.R.; Frattasi, S.; Sørensen, T.B.; Mogensen, P.E.; Pajukoski, K. On the Feasibility of Precoded Single User MIMO for LTE-A Uplink. *JCM* **2009**, *4*, 155–163. [CrossRef]

73. Priyanto, B.E.; Codina, H.; Rene, S.; Sorensen, T.B.; Mogensen, P. Initial performance evaluation of DFT-spread OFDM based SC-FDMA for UTRA LTE uplink. In Proceedings of the 2007 IEEE 65th Vehicular Technology Conference-VTC2007-Spring, Dublin, Ireland, 22–25 April 2007; pp. 3175–3179.

74. Torres, P.; Gusmao, A. Detection issues with many BS antennas available for bandwidth-efficient uplink transmission in a MU-MIMO system. In Proceedings of the 2016 IEEE Wireless Communications and Networking Conference, Doha, Qatar, 3–6 April 2016; pp. 1–6.

75. Sun, Y.; Wang, J.; He, L.; Song, J. Spectral efficiency analysis for spatial modulation in massive MIMO uplink over dispersive channels. In Proceedings of the 2017 IEEE International Conference on Communications (ICC), Paris, France, 21–25 May 2017; pp. 1–6.

76. De Temiño, L.Á.M.R.; Berardinelli, G.; Frattasi, S.; Pajukoski, K.; Mogensen, P. Single-user MIMO for LTE-A uplink: Performance evaluation of OFDMA vs. SC-FDMA. In Proceedings of the 2009 IEEE Radio and Wireless Symposium, San Diego, CA, USA, 18–22 January 2009; pp. 304–307.

77. Berardinelli, G.; de Temino, L.A.M.R.; Frattasi, S.; Rahman, M.I.; Mogensen, P. OFDMA vs. SC-FDMA: Performance comparison in local area IMT-A scenarios. *IEEE Wirel. Commun.* **2008**, *15*, 64. [CrossRef]

78. Yang, H. A road to future broadband wireless access: MIMO-OFDM-based air interface. *IEEE Commun. Mag.* **2005**, *43*, 53–60. [CrossRef]

79. Clerckx, B.; Joudeh, H.; Hao, C.; Dai, M.; Rassouli, B. Rate splitting for MIMO wireless networks: A promising PHY-layer strategy for LTE evolution. *IEEE Commun. Mag.* **2016**, *54*, 98–105. [CrossRef]

80. Qualcomm Technologies, I. 5G Waveform & Multiple Access Techniques. Available online: https://www.qualcomm.com/media/documents/files/5g-research-on-waveform-and-multiple-access-techniques.pdf (accessed on 1 March 2022).

81. Rammyaa, B.; Vishvaksenan, K.S.; Poobal, S.; Krishnan, M.M.M. Coded downlink MIMO MC-CDMA system for cognitive radio network: Performance results. *Clust. Comput.* **2018**, *22*, 8371–8378. [CrossRef]

82. Han, S.; Guo, C.; Meng, W.; Li, C.; Cui, Y.; Tang, W. The uplink and downlink design of MIMO-SCMA system. In Proceedings of the 2016 International Wireless Communications and Mobile Computing Conference (IWCMC), Paphos, Cyprus, 5–9 September 2016; pp. 56–60.

83. Hadjer, B.; Abdelhafid, B. Comparison & Performance Evaluation of MIMO-FBMC and MIMO-UFMC systems for various equalization techniques. In Proceedings of the 2019 International Conference on Networking and Advanced Systems (ICNAS), Annaba, Algeria, 26–27 June 2019; pp. 1–5.

84. Zayani, R.; Shaiek, H.; Cheng, X.; Fu, X.; Alexandre, C.; Roviras, D. Experimental Testbed of post-OFDM Waveforms Toward Future Wireless Networks. *IEEE Access* **2018**, *6*, 67665–67680. [CrossRef]

85. Mauricio, W.V.; Araujo, D.C.; Neto, F.H.C.; Lima, F.R.M.; Maciel, T.F. A Low Complexity Solution for Resource Allocation and SDMA Grouping in Massive MIMO Systems. In Proceedings of the 2018 15th International Symposium on Wireless Communication Systems (ISWCS), Lisbon, Portugal, 28–31 August 2018; pp. 1–6.

86. Wu, S.; Zuo, R.; Zhang, W.; Song, Y. Successive-Parallel Interference Cancellation Multi-user Detection Algorithm for MUSA Uplink. In *Wireless and Satellite Systems, Proceedings of the 10th EAI International Conference, WiSATS 2019, Harbin, China, 12–13 January 2019*; Springer: Cham, Switzerland, 2019; pp. 541–551.

87. Ding, Z.; Schober, R.; Poor, H.V. A General MIMO Framework for NOMA Downlink and Uplink Transmission Based on Signal Alignment. *IEEE Trans. Wirel. Commun.* **2016**, *15*, 4438–4454. [CrossRef]

88. Zayani, R.; Medjahdi, Y.; Shaiek, H.; Roviras, D. WOLA-OFDM: A potential candidate for asynchronous 5G. In Proceedings of the 2016 IEEE Globecom Workshops (GC Wkshps), Washington, DC, USA, 4–8 December 2016; pp. 1–5.

89. Ahmed, R.; Schaich, F.; Wild, T. OFDM Enhancements for 5G Based on Filtering and Windowing. In *Multiple Access Techniques for 5G Wireless Networks and Beyond*; Springer: Berlin/Heidelberg, Germany, 2019; pp. 39–61.

90. Jiang, T.; Chen, D.; Ni, C.; Qu, D. (Eds.) Chapter 1—Introduction. In *OQAM/FBMC for Future Wireless Communications*; Academic Press: Cambridge, MA, USA, 2018; pp. 1–24.

91. Goztepe, C.; Kurt, G.K. The impact of out of band emissions: A measurement based performance comparison of UF-OFDM and CP-OFDM. *Phys. Commun.* **2019**, *33*, 78–89. [CrossRef]

92. Chen, X.; Zhang, S.; Zhang, A. On MIMO-UFMC in the Presence of Phase Noise and Antenna Mutual Coupling. *Radio Sci.* **2017**, *52*, 1386–1394. [CrossRef]

93. Danneberg, M.; Michailow, N.; Gaspar, I.; Matthé, M.; Dan, Z.; Mendes, L.L.; Fettweis, G. Implementation of a 2 by 2 MIMO-GFDM transceiver for robust 5G networks. In Proceedings of the 2015 International Symposium on Wireless Communication Systems (ISWCS), Brussels, Belgium, 25–28 August 2015; IEEE: Piscataway, NJ, USA, 2015; pp. 236–240.

94. Zhang, W.; Zhang, Z.; Qi, L.; Dou, Z. Lattice-reduction-aided signal detection in spatial multiplexing MIMO–GFDM systems. *Phys. Commun.* **2019**, *33*, 71–77. [CrossRef]

95. Pereira de Figueiredo, F.A.; Aniceto, N.F.; Seki, J.; Moerman, I.; Fraidenraich, G. Comparing f-OFDM and OFDM Performance for MIMO Systems Considering a 5G Scenario. In Proceedings of the 5GWF2019, the the 2019 IEEE 2nd 5G World Forum, Dresden, Germany, 30 September–2 October 2019; pp. 1–6.

96. Caus, M.; Pérez-Neira, A.I. Transmitter-receiver designs for highly frequency selective channels in MIMO FBMC systems. *IEEE Trans. Signal Process.* **2012**, *60*, 6519–6532. [CrossRef]

97. Delmade, A.; Browning, C.; Farhang, A.; Marchetti, N.; Doyle, L.E.; Koilpillai, R.D.; Barry, L.P.; Venkitesh, D. Performance analysis of analog IF over fiber fronthaul link with 4G and 5G coexistence. *J. Opt. Commun. Netw.* **2018**, *10*, 174–182. [CrossRef]

98. Chang, Y.-K.; Ueng, F.-B. A novel turbo GFDM-IM receiver for MIMO communications. *AEU Int. J. Electron. Commun.* **2018**, *87*, 22–32. [CrossRef]

99. Sharief, A.H.; Sairam, M.S. Performance analysis of MIMO-RDWT-OFDM system with optimal genetic algorithm. *AEU Int. J. Electron. Commun.* **2019**, *111*, 152912. [CrossRef]

100. Singh, A.; Naik, K.K.; Kumar, C.R.S. NOMURA: A Spectrally Efficient Non-orthogonal 5G Multiple Access Downlink Scheme for Cognitive Radio. *IETE Tech. Rev.* **2018**, *37*, 1–10. [CrossRef]

101. Zakaria, R.; Le Ruyet, D. A novel filter-bank multicarrier scheme to mitigate the intrinsic interference: Application to MIMO systems. *IEEE Trans. Wirel. Commun.* **2012**, *11*, 1112–1123. [CrossRef]

102. Zhao, Z.; Gong, X.; Schellmann, M. A Novel FBMC/OQAM Scheme Facilitating MIMO FDMA without the Need for Guard Bands. In Proceedings of the WSA 2016 20th International ITG Workshop on Smart Antennas, Munich, Germany, 9–11 March 2016; pp. 1–5.

103. Yu, X.; Guanghui, Y.; Xiao, Y.; Zhen, Y.; Jun, X.; Bo, G. FB-OFDM: A novel multicarrier scheme for 5G. In Proceedings of the 2016 European Conference on Networks and Communications (EuCNC), Athens, Greece, 27–30 June 2016; pp. 271–276.

104. Jin, C.; Hu, S.; Huang, Y.; Li, F.; Zhang, J.; Ma, S. On design of conjugated transmission scheme for FBMC/OQAM systems with interference cancellation. *China Commun.* **2017**, *14*, 166–175. [CrossRef]

105. Aminjavaheri, A.; Farhang, A.; Rezazadehreyhani, A.; Doyle, L.E.; Farhang-Boroujeny, B. OFDM without CP in massive MIMO. *IEEE Trans. Wirel. Commun.* **2017**, *16*, 7619–7633. [CrossRef]

106. Pereira, A.; Bento, P.; Gomes, M.; Dinis, R.; Silva, V. TIBWB-OFDM: A Promising Modulation Technique for MIMO 5G Transmissions. In Proceedings of the 2018 IEEE 88th Vehicular Technology Conference (VTC-Fall), Chicago, IL, USA, 27–30 August 2018; IEEE: Piscataway, NJ, USA, 2018; pp. 1–5.

107. Başar, E.; Ü, A.; Panayırcı, E.; Poor, H.V. Orthogonal Frequency Division Multiplexing With Index Modulation. *IEEE Trans. Signal Process.* **2013**, *61*, 5536–5549. [CrossRef]

108. Tarrab, M.; Feuer, A. Convergence and performance analysis of the normalized LMS algorithm with uncorrelated Gaussian data. *IEEE Trans. Inf. Theory* **1988**, *34*, 680–691. [CrossRef]

109. Simon, E.P.; Khalighi, M.A. Iterative soft-Kalman channel estimation for fast time-varying MIMO-OFDM channels. *IEEE Wirel. Commun. Lett.* **2013**, *2*, 599–602. [CrossRef]

110. Kim, K.; Kalantarova, N.; Kozat, S.S.; Singer, A.C. Linear MMSE-optimal turbo equalization using context trees. *IEEE Trans. Signal Process.* **2013**, *61*, 3041–3055. [CrossRef]

111. Meredith, J.M. Study on downlink multiuser superposition transmission for LTE. In Proceedings of the TSG RAN Meeting, Tokyo, Japan, 9–11 March 2015.

112. Tseng, C.; Cheng, Y.; Chung, C. Subspace-Based Blind Channel Estimation for OFDM by Exploiting Cyclic Prefix. *IEEE Wirel. Commun. Lett.* **2013**, *2*, 691–694. [CrossRef]

113. Yin, C.; Li, J.; Hou, X.; Yue, G. Pilot aided LS channel estimation in MIMO-OFDM systems. In Proceedings of the 2006 8th International Conference on Signal Processing, Guilin, China, 16–20 November 2006.

114. He, C.; Tian, C.; Li, X.; Zhang, C.; Zhang, S.; Liu, C. A channel estimation scheme for MIMO-OFDM systems. *J. Phys. Conf. Ser.* **2017**, *887*, 012039. [CrossRef]

115. Tang, R.; Zhou, X.; Wang, C. Singular Value Decomposition Channel Estimation in STBC MIMO-OFDM System. *Appl. Sci.* **2019**, *9*, 3067. [CrossRef]

116. Li, W.; Wang, X.; Gu, P.; Wang, D. Research on Channel Estimation of MIMO–OFDM System. In *Informatics and Management Science III*; Springer: Berlin/Heidelberg, Germany, 2013; pp. 67–73.

117. Zheng, K.; Su, J.; Wang, W. Iterative DFT-based Channel Estimation for MIMO-OFDM Systems. In Proceedings of the 2006 International Conference on Communications, Circuits and Systems, Hangzhou, China, 25–28 June 2006; IEEE: Piscataway, NJ, USA, 2006; pp. 1081–1085.

118. Sure, P.; Bhuma, C.M. A pilot aided channel estimator using DFT based time interpolator for massive MIMO-OFDM systems. *AEU Int. J. Electron. Commun.* **2015**, *69*, 321–327. [CrossRef]

119. Dai, L.; Wang, Z.; Yang, Z. Spectrally efficient time-frequency training OFDM for mobile large-scale MIMO systems. *IEEE J. Sel. Areas Commun.* **2013**, *31*, 251–263. [CrossRef]

120. Carbonelli, C.; Franz, S. Performance analysis of MIMO OFDM ML detection in the presence of channel estimation error. In Proceedings of the 2008 IEEE 10th International Symposium on Spread Spectrum Techniques and Applications, Bologna, Italy, 25–28 August 2008; pp. 692–697.

121. Hlaing, M.; Al-Dhahir, N.; Yinghui, L. Optimal training signals for MIMO OFDM channel estimation in the presence of frequency offset and phase noise. *IEEE Trans. Commun.* **2006**, *54*, 1754–1759. [CrossRef]

122. Hardjawana, W.; Li, R.; Vucetic, B.; Li, Y.; Yang, X. A new iterative channel estimation for high mobility MIMO-OFDM systems. In Proceedings of the 2010 IEEE 71st Vehicular Technology Conference, Taipei, Taiwan, 16–19 May 2010; pp. 1–5.

123. Mishra, A.; Yashaswini, N.S.; Jagannatham, A.K. SBL-Based Joint Sparse Channel Estimation and Maximum Likelihood Symbol Detection in OSTBC MIMO-OFDM Systems. *IEEE Trans. Veh. Technol.* **2018**, *67*, 4220–4232. [CrossRef]

124. Motade, S.N.; Kulkarni, A.V. Channel Estimation and Data Detection Using Machine Learning for MIMO 5G Communication Systems in Fading Channel. *Technologies* **2018**, *6*, 72. [CrossRef]

125. Chen, Y.-S.; Wu, J.-Y. Statistical covariance-matching based blind channel estimation for zero-padding MIMO–OFDM systems. *EURASIP J. Adv. Signal Process.* **2012**, *2012*, 139. [CrossRef]

126. Chen, Y.-S.; Song, J.-H. Semiblind channel estimation for MIMO–OFDM systems. *EURASIP J. Adv. Signal Process.* **2012**, *2012*, 212. [CrossRef]

127. Wan, F.; Zhu, W.-P.; Swamy, M. An enhanced scheme for second-order-statistics estimation in MIMO-OFDM systems. In Proceedings of the 2009 IEEE International Symposium on Circuits and Systems, Taipei, Taiwan, 24–27 May 2009; pp. 701–704.

128. Bhandari, R.; Jadhav, S. Novel Spectral Efficient Technique for MIMO-OFDM Channel Estimation with Reference to PAPR and BER Analysis. *Wirel. Pers. Commun.* **2019**, *104*, 1227–1242. [CrossRef]

129. Peken, T.; Vanhoy, G.; Bose, T. Blind channel estimation for massive MIMO. *Analog. Integr. Circuits Signal Process.* **2017**, *91*, 257–266. [CrossRef]

130. Wang, K.; Gan, Z.; Liu, J.; He, W.; Xu, S. Deterministic compressed sensing based channel estimation for MIMO OFDM systems. *Clust. Comput.* **2019**, *22*, 2971–2980. [CrossRef]

131. Hedayati, M.K.; Bakhshi, H.; Cheraghi, M. SAGE algorithm for semi-blind channel estimation and symbol detection for STBC MIMO OFDM systems. *Wirel. Pers. Commun.* **2013**, *71*, 1541–1555. [CrossRef]

132. Mawatwal, K.; Sen, D.; Roy, R. A Semi-Blind Channel Estimation Algorithm for Massive MIMO Systems. *IEEE Wirel. Commun. Lett.* **2017**, *6*, 70–73. [CrossRef]

133. Jeya, R.; Amutha, B. Optimized semiblind sparse channel estimation algorithm for MU-MIMO OFDM system. *Comput. Commun.* **2019**, *146*, 103–109. [CrossRef]

134. Tang, L.; Abu-Rgheff, M.A. Joint Pilot-Aided and Blind Decision-Directed Channel Estimation for MIMO-OFDM System. In Proceedings of the 2007 IEEE 18th International Symposium on Personal, Indoor and Mobile Radio Communications, Athens, Greece, 3–7 September 2007; pp. 1–5.

135. Park, S.; Choi, J.W.; Lee, K.; Shim, B. Soft decision-directed channel estimation for multiuser MIMO systems. In Proceedings of the 2015 IEEE 26th Annual International Symposium on Personal, Indoor and Mobile Radio Communications (PIMRC), Hong Kong, China, 30 August–2 September 2015; IEEE: Piscataway, NJ, USA, 2015; pp. 95–99.

136. Park, S.; Shim, B.; Choi, J.W. Iterative channel estimation using virtual pilot signals for MIMO-OFDM systems. *IEEE Trans. Signal Process.* **2015**, *63*, 3032–3045. [CrossRef]

137. Yoon, D.; Moon, J. Soft-decision-directed MIMO channel estimation geared to pipelined turbo receiver Architecture. In Proceedings of the 2010 IEEE International Conference on Communications, Cape Town, South Africa, 23–27 May 2010; pp. 1–6.

138. Mehrabi, M.; Mohammadkarimi, M.; Ardakani, M.; Jing, Y. Decision Directed Channel Estimation Based on Deep Neural Network k-step Predictor for MIMO Communications in 5G. *arXiv* **2019**, arXiv:1901.03435. [CrossRef]

139. Ketonen, J.; Juntti, M.; Ylioinas, J.; Cavallaro, J.R. Implementation of LS, MMSE and SAGE channel estimators for mobile MIMO-OFDM. In Proceedings of the 2012 Conference Record of the Forty 6th Asilomar Conference on Signals, Systems and Computers (ASILOMAR), Pacific Grove, CA, USA, 4–7 November 2012; pp. 1092–1096.

140. Coleri, S.; Ergen, M.; Puri, A.; Bahai, A. Channel estimation techniques based on pilot arrangement in OFDM systems. *IEEE Trans. Broadcast.* **2002**, *48*, 223–229. [CrossRef]

141. Xie, H.; Andrieux, G.; Wang, Y.; Diouris, J.-F.; Feng, S. Efficient time domain threshold for sparse channel estimation in OFDM system. *AEU Int. J. Electron. Commun.* **2014**, *68*, 277–281. [CrossRef]

142. Belgiovine, M.; Sankhe, K.; Bocanegra, C.; Roy, D.; Chowdhury, K.R. Deep learning at the edge for channel estimation in beyond-5G massive MIMO. *IEEE Wirel. Commun.* **2021**, *28*, 19–25. [CrossRef]

143. Kirik, M.; HAMAMREH, J.M. Interference Signal Superposition-aided MIMO with Antenna Number Modulation and Adaptive Antenna Selection for Achieving Perfect Secrecy. *RS Open J. Innov. Commun. Technol.* **2021**, *2*, 1–11. [CrossRef]

144. Yang, S.; Kobayashi, M.; Piantanida, P.; Shamai, S. Secrecy degrees of freedom of MIMO broadcast channels with delayed CSIT. *IEEE Trans. Inf. Theory* **2013**, *59*, 5244–5256. [CrossRef]

145. Hyvarinen, A. Fast and robust fixed-point algorithms for independent component analysis. *IEEE Trans. Neural Netw.* **1999**, *10*, 626–634. [CrossRef] [PubMed]

146. Immanuvel, A.; Suganthi, M. Performance Analysis of Low Power Channel Estimator for Multi User MIMO-OFDM System. *Wirel. Pers. Commun.* **2019**, *107*, 341–350. [CrossRef]

147. Gao, J.; Zhu, X.; Nandi, A.K. Non-redundant precoding and PAPR reduction in MIMO OFDM systems with ICA based blind equalization. *IEEE Trans. Wirel. Commun.* **2009**, *8*, 3038–3049.

148. Chen, B.-S.; Yang, C.-Y.; Liao, W.-J. Robust fast time-varying multipath fading channel estimation and equalization for MIMO-OFDM systems via a fuzzy method. *IEEE Trans. Veh. Technol.* **2012**, *61*, 1599–1609. [CrossRef]

149. Chang, Y.-K.; Ueng, F.-B.; Shen, Y.-S.; Liao, C.-H. Joint channel estimation and turbo equalisation for MIMO-OFDM-IM systems. *Int. J. Electron.* **2019**, *106*, 721–740. [CrossRef]

150. Chen-Hu, K.; Armada, A.G. Low-Complexity Computation of Zero-Forcing Equalizers for Massive MIMO-OFDM. In Proceedings of the 2019 IEEE 89th Vehicular Technology Conference (VTC2019-Spring), Kuala Lumpur, Malaysia, 28 April–1 May 2019; IEEE: Piscataway, NJ, USA, 2019; pp. 1–5.

151. Chu, L.; Li, H.; Qiu, R.C. LEMO: Learn to Equalize for MIMO-OFDM Systems with Low-Resolution ADCs. *arXiv* **2019**, arXiv:1905.06329.

152. Pereira, A.; Bento, P.; Gomes, M.; Dinis, R.; Silva, V. Iterative MRC and EGC Receivers for MIMO-OFDM Systems. In Proceedings of the 2018 IEEE 87th Vehicular Technology Conference (VTC Spring), Porto, Portugal, 3–6 June 2018; pp. 1–4.

153. Chern, S.; Chen, J.; Wu, C. Novel frequency-domain DFE equalizer with oblique projection for CP-free space-time block coded MIMO-OFDM systems. In Proceedings of the 2009 International Symposium on Intelligent Signal Processing and Communication Systems (ISPACS), Kanazawa, Japan, 7–9 January 2009; IEEE: Piscataway, NJ, USA, 2009; pp. 541–545.

154. Ma, S.; Ng, T.-S. Semi-blind time-domain equalization for MIMO-OFDM systems. *IEEE Trans. Veh. Technol.* **2008**, *57*, 2219–2227.

155. Noori, K.; Haider, S.A. Channel Equalization of MIMO OFDM system using RLS Algorithm. In Proceedings of the 2007 International Conference on Wireless Communications, Networking and Mobile Computing, Shanghai, China, 21–25 September 2007; pp. 160–163.

156. Boher, L.; Rabineau, R.; Hélard, M. An Efficient MMSE Equalizer Implementation for 4 × 4 MIMO-OFDM Systems in Frequency Selective Fast Varying Channels. In Proceedings of the 2007 IEEE 18th International Symposium on Personal, Indoor and Mobile Radio Communications, Athens, Greece, 3–7 September 2007; pp. 1–5.